The Astrophysical Journal, 702:226–248, 2009 September 1 doi:10.1088/0004-637X/702/1/226

FROM SHOCK BREAKOUT TO PEAK AND BEYOND: EXTENSIVE PANCHROMATIC OBSERVATIONS OF THE TYPE Ib SUPERNOVA 2008D ASSOCIATED WITH *SWIFT* X-RAY TRANSIENT 080109

M. Modjaz[1,19], W. Li[1], N. Butler[1,20], R. Chornock[1], D. Perley[1], S. Blondin[2,3], J. S. Bloom[1,4,21], A. V. Filippenko[1], R. P. Kirshner[3], D. Kocevski[1], D. Poznanski[1], M. Hicken[3], R. J. Foley[1,3,22], G. S. Stringfellow[5], P. Berlind[3], D. Barrado y Navascues[6], C. H. Blake[3], H. Bouy[1,7], W. R. Brown[3], P. Challis[3], H. Chen[8], W. H. de Vries[9,10], P. Dufour[11], E. Falco[3], A. Friedman[3], M. Ganeshalingam[1], P. Garnavich[12], B. Holden[13], G. Illingworth[13], N. Lee[1], J. Liebert[11], G. H. Marion[14], S. S. Olivier[15], J. X. Prochaska[13], J. M. Silverman[1], N. Smith[1], D. Starr[1,4], T. N. Steele[1], A. Stockton[16], G. G. Williams[17] , and W. M. Wood-Vasey[18]

[1] Department of Astronomy, University of California, Berkeley, CA 94720-3411, USA; mmodjaz@astro.berkeley.edu
[2] European Southern Observatory (ESO), Karl-Schwarzschild-Str. 2, D-85748 Garching, Germany
[3] Harvard-Smithsonian Center for Astrophysics, 60 Garden Street, Cambridge, MA, 02138, USA
[4] Las Cumbres Global Telescope Network, 6740 Cortona Dr., Santa Barbara, CA 93117, USA
[5] Center for Astrophysics & Space Astronomy, University of Colorado, Boulder, CO 80309-0389, USA
[6] LAEX, Centro de Astrobiología, (INTA-CSIC), Apdo. 78, E-28691 Villanueva de la Cañada (Madrid), Spain
[7] Instituto de Astrofisica de Canarias, C/Via Lactea S/N, E-38205 La Laguna, Tenerife, Spain
[8] Department of Astronomy, University of Chicago, 5640 South Ellis Avenue, Chicago, IL 60637, USA
[9] University of California, Department of Physics, 1 Shields Ave, Davis, CA 95616, USA
[10] Institute for Geophysics and Planetary Physics, LLNL, L-413, 7000 East Avenue, Livermore, CA 94550, USA
[11] Department of Astronomy, University of Arizona, 933 N. Cherry Ave. Tucson, AZ 85721, USA
[12] Department of Physics, 225 Nieuwland Science Hall, University of Notre Dame, Notre Dame, IN 46556, USA
[13] University of California Observatories – Lick Observatory, University of California, Santa Cruz, CA 95064, USA
[14] Astronomy Department, University of Texas at Austin, Austin, TX 78712, USA
[15] Lawrence Livermore National Laboratory, 7000 East Avenue, Livermore, CA 94550, USA
[16] Institute for Astronomy, University of Hawaii, 2680 Woodlawn Drive, Honolulu, HI 96822, USA
[17] Steward Observatory, University of Arizona, 933 North Cherry Avenue, Tucson, AZ 85721, USA
[18] Department of Physics & Astronomy, 3941 O'Hara St, University of Pittsburgh, Pittsburgh, PA 15260, USA
Received 2008 May 18; accepted 2009 June 18; published 2009 August 10

ABSTRACT

We present extensive early photometric (ultraviolet through near-infrared) and spectroscopic (optical and near-infrared) data on supernova (SN) 2008D as well as X-ray data analysis on the associated *Swift* X-ray transient (XRT) 080109. Our data span a time range of 5 hr before the detection of the X-ray transient to 150 days after its detection, and a detailed analysis allowed us to derive constraints on the nature of the SN and its progenitor; throughout we draw comparisons with results presented in the literature and find several key aspects that differ. We show that the X-ray spectrum of XRT 080109 can be fit equally well by an absorbed power law or a superposition of about equal parts of both power law and blackbody. Our data first established that SN 2008D is a spectroscopically normal SN Ib (i.e., showing conspicuous He lines) and showed that SN 2008D had a relatively long rise time of 18 days and a modest optical peak luminosity. The early-time light curves of the SN are dominated by a cooling stellar envelope (for $\Delta t \approx 0.1$–4 days, most pronounced in the blue bands) followed by ^{56}Ni decay. We construct a reliable measurement of the bolometric output for this stripped-envelope SN, and, combined with estimates of $E_{\rm K}$ and $M_{\rm ej}$ from the literature, estimate the stellar radius $R_\star$ of its probable Wolf–Rayet progenitor. According to the model of Waxman et al. and Chevalier & Fransson, we derive $R_\star^{\rm W07} = 1.2 \pm 0.7 R_\odot$ and $R_\star^{\rm CF08} = 12 \pm 7\ R_\odot$, respectively; the latter being more in line with typical WN stars. Spectra obtained at three and four months after maximum light show double-peaked oxygen lines that we associate with departures from spherical symmetry, as has been suggested for the inner ejecta of a number of SN Ib cores.

Key words: galaxies: distances and redshifts – galaxies: individual (NGC 2770) – supernovae: general – supernovae: individual (SN 2008D)

Online-only material: color figures, machine-readable table

1. INTRODUCTION

The connection between long-duration gamma-ray bursts (GRBs) and broad-lined Type Ic supernovae (SNe Ic-bl) has recently piqued interest in certain SNe as GRB progenitors (see Woosley & Bloom 2006 for a review). A few SNe connected with GRBs have been fairly well observed, but there exists little early-time and high-energy data on the comparison set of core-collapse SNe.

Massive stars (initial mass $M \gtrsim 8\ M_\odot$) die violently, and the ensuing core-collapse SNe are classified into different spectroscopic SN subtypes. The classification depends on the presence or absence of hydrogen and helium in the SN spectra, and its sequence is set by the amount and kind of outer envelopes the progenitor retained before explosion: Type II SNe show prominent H, while Type IIb SNe show He and weaker H, Type Ib SNe lack obvious H and conspicuously show He (but see Branch et al. 2006), and Type Ic SNe lack both H and obvious He (see Filippenko 1997 for a review). SNe IIb, Ib, and Ic are

[19] Miller Fellow
[20] GLAST/Einstein Fellow
[21] Sloan Research Fellow
[22] Clay Fellow

collectively called "stripped-envelope SNe" (Clocchiatti et al. 1996). While the number of well observed, normal, stripped-envelope SNe has grown in the past decade (see Matheson et al. 2001; Richardson et al. 2006; Modjaz 2007 and references therein), there are few observations at very early times after the collapse, especially when the shock breaks out of the stellar envelope (Campana et al. 2006; Gezari et al. 2008; Schawinski et al. 2008).

Recently, the *Swift* satellite (Gehrels et al. 2004) with its rapid slewing capabilities, space-based nature, and X-ray and optical/ultraviolet telescopes has opened a new window for SN observations soon after their massive progenitors explode. A marvelous opportunity to closely study the shock breakout and the evolution of a nearby SN was offered by X-ray transient (XRT) 080109/SN 2008D. During the *Swift* follow-up observations of SN 2007uy (Nakano et al. 2008; Blondin et al. 2008c) in NGC 2770, XRT 080109 was discovered serendipitously (Berger & Soderberg 2008; Kong & Maccarone 2008; Soderberg et al. 2008b) in the same galaxy in data obtained with the *Swift* X-ray telescope (*Swift*/XRT), starting on 2008 January 9.56 (UT dates are used throughout this paper).

After the announcement of the XRT detection, numerous groups obtained data on the optical counterpart (see Page et al. 2008; Soderberg et al. 2008b, and Malesani et al. 2009 for a detailed account), which revealed it to be an SN. From spectra, Soderberg et al. (2008a) reported a featureless continuum with a suggestion of a broad bump near 5500 Å, possibly indicating an SN feature, and Malesani et al. (2008) originally classified the optical transient as an SN Ib/c via its lack of H; Blondin et al. (2008a) and Valenti et al. (2008b) then classified the transient as an SN Ic possibly with broad spectral lines. Then we (Modjaz et al. 2008a) were the first to suggest a classification as a spectroscopically ordinary SN Ib, a classification supported by subsequent reports (Valenti et al. 2008a; Soderberg et al. 2008b; Mazzali et al. 2008; Malesani et al. 2009). We promptly established an extensive monitoring program of SN 2008D with facilities at Mt. Hopkins and Lick Observatory, extending the observing campaign that was already underway for SN 2007uy in the same galaxy. Spectra and photometry were obtained on a nightly basis (weather permitting) starting 2008 January 10, sometimes with multiple observations per night. In addition, we reduced and analyzed public *Swift*/XRT and *Swift*/UVOT data, as well as *Chandra* X-ray observations. Furthermore, we obtained optical spectra at the Apache Point Observatory through the awarding of Director's Discretionary Time.

The mechanism for removing progressively increasing amounts of the H and He layers in the progenitors of stripped-envelope SNe is not fully understood. The origin could either lie in strong winds of the very massive progenitor ($\gtrsim 30\ M_{\odot}$; Chiosi & Maeder 1986; Woosley et al. 1993), sudden eruptions (Smith & Owocki 2006), interactions with a binary companion star (e.g., Nomoto et al. 1995; Podsiadlowski et al. 2004), or the interplay of all the above. A larger set of SN data is needed to uncover trends between the underlying properties of progenitor radii, ejecta mass, and amount of ^{56}Ni produced (Richardson 2009).

In Section 2, we present X-ray data obtained with *Swift*/XRT and *Chandra* of XRT 080109 associated with SN 2008D, and in Sections 3 and 5 we present our extensive optical and near-infrared (NIR) photometry and spectroscopy on SN 2008D. Moreover, we present pre-explosion optical and NIR images from follow-up observations of SN 2007uy that were obtained 2.8 and 4.5 hr before the onset of XRT 080109, yielding stringent upper limits. We discuss the photometric properties of SN 2008D related to the two phases of evolution in Section 4 and construct bolometric light curves in Section 6. Section 7 compares it with the rest of the known SNe with observed shock breakout and emission from the stellar envelope, and Section 8 presents nebular spectra that reveal double-peaked oxygen lines, which we attribute to global core ejecta asphericities. In Section 9, we discuss in detail the X-ray properties of XRT 080109 compared with other kinds of X-ray events. We conclude with Section 10. Throughout we draw comparisons with results presented in the literature (Soderberg et al. 2008b; Mazzali et al. 2008; Chevalier & Fransson 2008; Malesani et al. 2009) and find several key aspects that differ. Unique aspects of our work include the very early-time (< 1 day after outburst) NIR data on SN 2008D, NIR spectra, and late-time optical spectra.

2. X-RAY PHOTOMETRY AND SPECTROSCOPY

Here, we discuss our independent reduction and analysis of the public *Swift* data and the *Chandra* data (PI Pooley; Pooley & Soderberg 2008) of XRT 080109. While separate reductions and analysis of the same raw data exist in the literature (Soderberg et al. 2008b; Li 2008; Mazzali et al. 2008; Xu et al. 2008), our analysis shows that the data are consistent with a range of combinations for the contributions of the blackbody and power-law contributions. Constraining the spectral shape of the X-ray emission and its components has ramifications for interpreting the X-ray emission mechanism and directly impacts the question of whether XRT 080109 was produced by a jet, as for one group (Mazzali et al. 2008) the amount of blackbody contribution, and thus the small derived value for blackbody X-ray emitting area, is a cornerstone for their jet interpretation of the origin of the X-ray emission.

We downloaded the *Swift*/BAT and *Swift*/XRT (Burrows et al. 2005) data from the *Swift* Archive.[23] The XRT data were processed with version 0.11.4 of the `xrtpipeline` reduction script from the HEAsoft 6.3.1[24] software release. We employed 2007 December 4 XRT calibration files. Our reduction of XRT data from cleaned event lists output by `xrtpipeline` to science-ready light curves and spectra is described in detail by Butler & Kocevski (2007a). In particular, our custom IDL tools account on a frame-by-frame basis for pileup and source flux lost due to hot or bad pixels and also perform rejection of pixels contaminated by nearby field sources.

In order to best account for contamination from nearby sources, we extract source flux in circular regions of two sizes: 16 and 4.4 pixels radius, corresponding to 90% and 50% source containment, respectively. The spectra were fit using ISIS.[25] Quoted uncertainties below correspond to 90% confidence intervals.

2.1. X-ray Photometry: A 520 s Transient

The X-ray transient (Berger & Soderberg 2008) rises in a time 50 ± 30 s, and has a duration $T_{90} = 470 \pm 30$ s or $\Delta t_{\rm FWHM} = 80 \pm 30$ s. Consistent with Soderberg et al. (2008b), we adopt $t_0 =$ 2008-01-09 13:32:49 ($\pm$ 5 s) as the time of onset of the XRT, i.e., the start of the *Swift*/XRT observations.

In Figure 1, we plot the X-ray light curve of XRT 080109/SN 2008D, after adequately subtracting the other three X-ray field sources as resolved by *Chandra* observations (Pooley &

[23] ftp://legacy.gsfc.nasa.gov/swift/data
[24] http://heasarc.gsfc.nasa.gov/docs/software/lheasoft/
[25] http://space.mit.edu/CXC/ISIS/

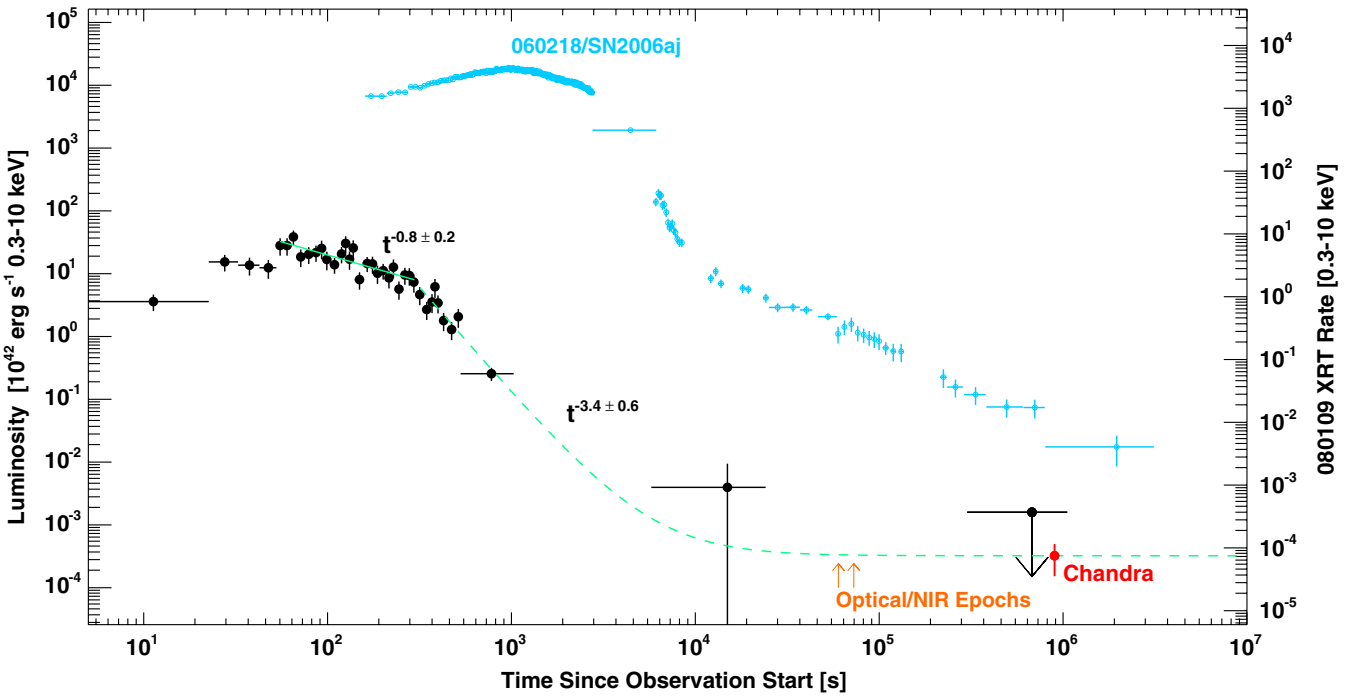

Figure 1. Observed temporal evolution of the X-ray luminosity of XRT 080109/SN 2008D (black points) in the XRT bands (0.3–10 keV), since t_0 = 2008-01-09 13:32:49, including the *Chandra* observation from 2008 January 19. Depending on when one defines the time of onset, a range of power-law slopes (the green line) can be fit with $\alpha = -3.4 \pm 0.6$ (where $L_X \propto t^{\alpha}$) for data after ∼300 s. We adopt the count rate to luminosity conversion from the power-law fit to the spectrum, which is 4.3×10^{42} erg s^{-1} per count s^{-1}. The epochs on which optical and NIR data were obtained are indicated. See text for details. For comparison, we also plot the *Swift* X-ray light curve of XRF 060218/SN 2006aj (blue points, Campana et al. 2006; Butler et al. 2006), which *Swift*/XRT started observing ∼100 s after the gamma-ray trigger.

(A color version of this figure is available in the online journal.)

Soderberg 2008; see below). Prior to 1 ks but after the peak time, the X-ray luminosity (L_X) decay can be fit by a broken power law in time with late-time index $\alpha = -3.4 \pm 0.6$ (where $L_X \propto t^{\alpha}$), while data taken $\Delta t \lesssim 300$ s are best described by a decaying power law with $\alpha = -0.8 \pm 0.2$. For comparison, we plot in Figure 1 the X-ray light curve of XRF 060218/SN 2006aj, the most recent GRB/XRF-SN (Campana et al. 2006; Mirabal et al. 2006; Modjaz et al. 2006; Pian et al. 2006; Sollerman et al. 2006), which was discovered by *Swift* (Campana et al. 2006; Butler et al. 2006). While the expression "X-ray flash" (XRF, see Heise et al. 2001) is used in the literature when referring to the high-energy event 060218, the transient 060218 was qualitatively different from classical X-ray flashes, in that it likely exhibited a shock breakout component (Campana et al. 2006; Waxman et al. 2007). In Section 9, we discuss in detail the properties of the peculiar XRF 060218 and XRT 080109 compared to other classical XRFs.

The peak X-ray luminosity of XRT 080109 is ∼700 times lower than that of XRF 060218 associated with SN 2006aj. The fluence of the X-ray transient is about 3.0×10^{-8}erg cm^{-2} in the 2–10 keV band (3.7×10^{-8} erg cm^{-2} in the 2–18 keV band), where we have adopted the count-rate conversion for the pure power-law spectral fit (see Section 2.2) of 4.0×10^{-11} erg cm^{-2} s^{-1} per count s^{-1} which corresponds to 4.3×10^{42} erg s^{-1} per count s^{-1} for the adopted distance to XRT 080109 of $D = 31$ Mpc.

Chandra observations (Pooley & Soderberg 2008; Soderberg et al. 2008b) have shown that three bright field sources lie near the X-ray transient and likely contribute substantial counts at late times even for small *Swift*/XRT extraction regions. These sources (X1, X2, and X3; see Pooley & Soderberg 2008) are 3.″8, 1.″4, and 2.″6 (9.0, 3.2, and 6.1 XRT pixels), respectively, from the X-ray transient. Using the *Chandra* spectral fitting results and the *Swift*/XRT point-spread function (PSF) from the calibration database, we determine a field source contamination count rate of 2×10^{-3} (6.9×10^{-4}) counts s^{-1} for the 16 (4.4) pixel extraction region.

Correcting to the true source flux level using the PSF model shows that the flux from XRT 080109 (Figure 1) is dominated by the field source flux for any observations that start 5 ksec after t_0 (i.e., the data point at 16 ksec) and is likely completely overwhelmed by the field source flux after 1 day. We therefore use the 16 pixel extraction region for the temporal/spectral analysis prior to 5 ksecand the 4.4 pixel extraction region to measure or limit the flux at later times.

We determine the maximum-likelihood X-ray centroid position and frame offset relative to Sloan Digital Sky Survey (SDSS; $\Delta\alpha = 0.''8$ and $\Delta\delta = 2.''4$, using five X-ray/optical source matches) as described by Butler (2007b). Our best-fit XRT position is $\alpha = 09^h09^m30.78^s$, $\delta = +33°08'20.''1$ (±1.″6, J2000, 90% conf.), which is more uncertain than the optical position of SN 2008D with position end figures 30.65^s and 20.″3. These positions are consistent with those of Soderberg et al. (2008b). The X-ray light curve of XRT 080109 is given in Table 1.

2.2. X-ray Spectral Fitting: Power Law Versus Blackbody

We restrict our spectral fitting to the time period 0–520 s after the onset of XRT 080109, where the contamination from X-ray field sources is negligible (Pooley & Soderberg 2008).

Different groups, performing analysis of the same *Swift*/XRT data, come to different conclusions: Soderberg et al. (2008b) exclude an absorbed single blackbody (BB) fit on statistical grounds (with $\chi^2/\nu = 26.0/17$) and thus favor a simple power-

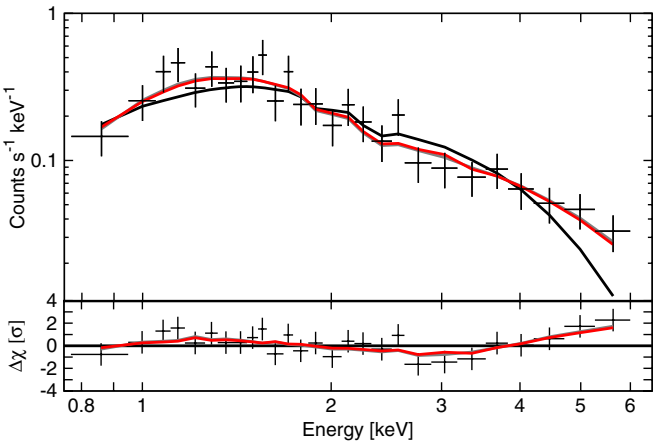

Figure 2. Observed X-ray spectrum of XRT 080109 (crosses) in the *Swift*/XRT bands (0.3–10 keV) averaged over the 520 s duration of the event. *Top*: best-fit blackbody (BB; the black solid line), power-law (PL; the dashed black line) and combined BB–PL (with equal contributions, the red solid line) models. Both the pure PL and the combined PL–BB models are excellent fits and are nearly indistinguishable. The combined PL–BB fit has different parameters than the individual pure PL and BB fits. *Bottom*: data residuals (crosses) from the BB model fit (the solid line), the PL model fit (the dashed line), and the combined BB–PL fit (the red solid line). The value for the deviation of the respective model fit from the data is the distance between the crosses and the respective lines.

(A color version of this figure is available in the online journal.)

law (PL) fit (with $\chi^2/\nu = 7.5/17$); Li (2008) argues that the data can be fit by an absorbed two-component BB fit (with $\chi^2/\nu = 10.4/16$) as well as by a pure PL fit, but excludes the two-component BB fit based on physical grounds arguing that the inferred BB radius (5×10^9 cm) is much smaller than the possible progenitor radius. Mazzali et al. (2008) claim that for any combined BB and PL fit, the BB contribution has to be small, namely at most 14% (whose fit gives $\chi^2/\nu = 20.6/21$), and that the implied small BB radius ($\sim 10^{10}$ cm) is evidence for a GRB jet (see also Section 9). However, we find that the low S/N data of XRT 080109 alone do not well constrain the contributions from a soft thermal excess and a harder PL continuum. In contrast to Mazzali et al. (2008), we find excellent fits ($\chi^2/\nu = 12.57/23$, see Figure 2.) for a *combined* BB–PL fit assuming a factor unity ratio of PL to bolometric BB flux (i.e., 50% bolometric contribution from a BB, see below) without increasing N_H relative to that in the pure PL fit ($\chi^2/\nu = 12.73/24$, $N_{\rm H} = 5.2^{+2.1}_{-1.8} \times 10^{21}$ cm^{-2}). This H-equivalent column density $N_{\rm H}$, which is greater than that expected from the Galaxy (1.7×10^{20} cm^{-2}; Dickey & Lockman 1990), is consistent with the large reddening value inferred from the optical-NIR data (Soderberg et al. 2008b, Section 6), given standard conversions between $N_{\rm H}$ and reddening (Predehl & Schmitt 1995).

For the combined BB–PL fit, the time-integrated PL photon index is $\Gamma = 2.1^{+0.3}_{-0.4}$ (where $N(E) \propto E^{-\Gamma}$), the BB temperature is $kT = 0.10 \pm 0.01$ keV and $R^{\rm X}_{\rm BB} = 10^{11}$ cm, i.e., a factor of 10 larger than computed by Mazzali et al. (2008). For comparison, the pure BB fit gives $\chi^2/\nu = 28.56/25$ with $R^{\rm X}_{\rm BB} = (1.0 \pm 0.2) \times 10^9$ cm and $kT = 0.75 \pm 0.07$ keV (Table 2). Hence, the apparent low $R^{\rm X}_{\rm BB}$ from the pure BB fit alone may be an artifact of incorrectly fitting a low signal-to-noise ratio (S/N) composite BB plus PL spectrum with just a pure BB model. For completeness, we list in Table 2 our *pure* BB and PL fits, whose parameters are broadly consistent with the analysis performed by the groups above; specifically, our pure PL fit gives a time-integrated photon index of $\Gamma = 2.1^{+0.3}_{-0.4}$.

Although the exact fraction of soft BB emission in XRT 080109 is poorly constrained by the data, a case can be made for the possible presence of BB emission through comparison to XRF 060218. The high-S/N X-ray spectrum of XRF 060218 during the proposed shock breakout phase at $t < 6$ ks was predominantly nonthermal but also required at high confidence a soft ($kT = 0.1$–0.2 keV) BB (Campana et al. 2006; Butler et al. 2006) with a ratio of about unity between PL and BB flux (Butler et al. 2006). If we downsample the spectrum of XRF 060218 for $t < 6$ ks to contain 380 counts as in XRT 080109, we find that the XRF 060218 spectrum is fit in a strikingly similar fashion to the XRT 080109 spectrum: a BB fit has $kT = 0.72^{+0.9}_{-0.5}$ keV and local $N_{\rm H} < 3.6 \times 10^{21}$ cm^{-2} ($\chi^2/\nu = 35.22/23$), while a PL fit has $\Gamma = 1.7 \pm 0.3$ and local $N_{\rm H} = 2.2^{+1.8}_{-1.5} \times 10^{21}$ cm^{-2} ($\chi^2/\nu = 9.25/23$). From the low χ^2/ν, we see that the PL

Table 1
X-ray Light Curve of XRT 080109

Δt (s)	δt (s)	Luminosity $L_{\rm x}$ (10^{42} erg s^{-1})	$\sigma_{(L_{\rm X})}$ (10^{42} erg s^{-1})
11.29	11.28	3.60	1.06
27.59	5.02	15.38	4.53
37.62	5.02	13.65	4.34
47.65	5.02	12.43	4.14
55.17	2.51	28.02	8.67
60.19	2.51	28.02	8.67
65.20	2.51	38.47	10.11
71.47	3.76	18.49	5.78
78.99	3.76	20.32	6.04
86.51	3.76	21.68	6.29
92.78	2.51	25.26	8.28
99.05	3.76	16.84	5.52
109.08	6.27	13.88	3.92
119.11	3.76	20.62	6.04
125.38	2.51	30.36	9.06
131.65	3.76	17.03	5.50
137.91	2.51	25.70	8.23
149.20	8.78	8.04	2.48
164.24	6.27	14.51	3.91
175.52	5.01	14.37	4.34
186.81	6.27	10.17	3.30
200.60	7.52	11.18	3.14
215.64	7.52	8.57	2.75
228.18	5.01	12.71	4.13
244.46	11.28	5.68	1.83
263.28	7.52	9.53	2.89
278.32	7.52	9.34	2.89
294.62	8.78	7.34	2.36
317.19	13.79	4.64	1.57
346.02	15.04	2.69	0.86
369.84	8.78	3.54	1.18
383.63	5.01	6.19	2.06
398.68	10.03	3.42	1.09
427.51	18.81	1.79	0.58
472.64	26.33	1.29	0.41
514.01	15.04	2.06	0.69
778.53	249.47	0.26	0.060
14944.11	9184.50	0.0040	0.0055
677205.64	376223.75	< 0.0016	...
898641.0[a]	17900	0.00032	0.00017

Notes. Using a count-to-luminosity conversion of 4.3×10^{42} erg s^{-1} per count s^{-1} based on the pure PL spectral fit, for a distance of $D = 31 \pm 2$ Mpc. *Swift* data unless noted otherwise.
[a] *Chanda* data.

Table 2
Model Parameters for X-ray Spectral Fits of XRT 080109

Parameter	Power-law (PL) Fit	Blackbody (BB) Fit	Combined PL+BB Fit[a]
Quality of Fit (χ^2/dof)	12.73/24	28.56/25	12.57/23
Implied $N_{\rm H}$ [10^{21} cm^{-2}]	$5.2^{+2.1}_{-1.8}$	< 1.5	$5.2^{+2.1}_{-1.8}$
Time-integrated Γ, kT, and [Γ;kT] respectively	$2.1^{+0.3}_{-0.4}$	0.75 ± 0.07	$2.1^{+0.3}_{-0.4}$; 0.10 ± 0.01
$L_{\rm X,iso}$[b] [10^{42} erg s^{-1}]	12^{+5}_{-2}	4.6 ± 0.6	13 ± 2[c]
$E_{\rm X,iso}$[b] [10^{45} erg]	5.8^{+2}_{-1}	2.4 ± 3	6.7 ± 4[c]

Notes.
[a] Assuming the same (factor unity) ratio of PL to BB flux as in XRF 060218 (Butler et al. 2006).
[b] Unabsorbed and time-averaged value over the range 0.3–10.0 keV (for PL fit) and bolometric (for BB fit), respectively, assuming $D = 31 \pm 2$ Mpc.
[c] Listed only for the BB component. $L_{\rm X,iso}$ and $E_{\rm X,iso}$ are computed assuming $R^{\rm X}_{\rm BB} = 10^{11}$ cm as required from the combined PL and BB fits.

model with $N_{\rm H}$ in excess of Galactic also effectively *overfits* the soft spectral excess in XRF 060218, which requires a PL plus BB given all the counts. We also note that the light curve of XRT 080109 is quite similar to that observed for XRF 060218/SN 2006aj, if we allow a time stretch by a factor of ∼0.1 (Figure 1). We discuss the implications and interpretation of the X-ray data in Section 9.

3. OPTICAL PHOTOMETRY

Optical photometry was obtained with the Katzman Automatic Imaging Telescope (KAIT; Filippenko et al. 2001) and the 1 m Nickel telescope, both at Lick Observatory, and the 1.2 m telescope at the Fred Lawrence Whipple Observatory (FLWO). We note that the host galaxy of SN 2008D, NGC 2770, was monitored by KAIT (Li & Filippenko 2008) during the regular course of the optical Lick Observatory Supernova Search (Filippenko et al. 2001; Filippenko 2005) as part of the nearby target galaxy sample, and that the regular SN detection software successfully detected this SN in data from 2008 January 11.42, which is 1.85 days after the X-ray outburst (Li & Filippenko 2008).

3.1. Photometric Calibrations

For photometric calibrations, the field of SN 2008D was observed in *UBVRI* during photometric nights on 2008 January 18, 19, and 20 with KAIT, in *BVRI* on 2008 January 12 with the Nickel 1 m telescope, and in $BVr'i'$ on 2008 January 18 with the FLWO 1.2 m telescope. About a dozen Landolt (1992) standard star fields were observed at different airmasses throughout each photometric night. Photometric solutions to the Landolt standard stars yield a scatter of ∼0.02 mag for all the filters for the Nickel telescope and about 0.03 mag for KAIT. The SN 2008D field was also observed for several sets of *UBVRI* images with different depth in the photometric nights. The photometric solutions are used to calibrate a set of local standard stars in the SN 2008D field as listed in Table 3, and a finder chart is shown in Figure 3. The calibration based on the FLWO 1.2 m telescope observations ("FLWO calibration") is consistent within the uncertainties with the Lick calibration (from the KAIT and Nickel telescopes) in the filters that they have in common (*BV*).

3.2. Lick Observatory Data Reduction

KAIT followed SN 2008D in *BVRI* and unfiltered mode nightly (weather permitting) after its discovery. As SN 2008D occurred on a spiral arm of NGC 2770, we use image subtraction

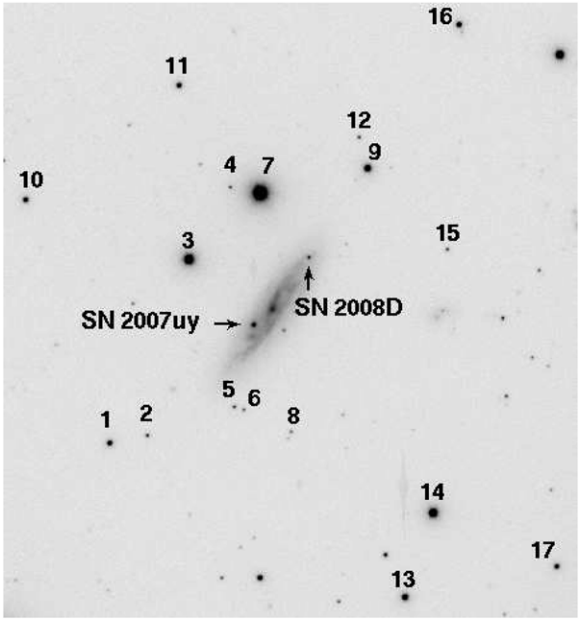

Figure 3. Finder chart for the local standard stars in the field of SN 2008D showing both SN 2008D and SN 2007uy in NGC 2770. The field of view is $10' \times 11'$. North is up and east is to the left. Displayed is the r'-band image taken with the FLWO 1.2 m telescope on 2008 January 29.

to remove the contamination of the host-galaxy emission. For template subtraction, we used pre-explosion images obtained with the FLWO 1.2 m telescope during the course of follow-up photometry for SN 2007uy, which also occurred in NGC 2770 (as shown in Figure 3).

For KAIT, the image subtraction and subsequent photometry reduction are performed with the KAIT photometry pipeline (M. Ganeshalingam et al. 2009, in preparation). Two independent image-subtraction routines were employed in the pipeline. One routine is based on the ISIS package (Alard & Lupton 1998) as modified by Brian Schmidt for the High-z Supernova Search Team (Riess et al. 1998), and the other is based on the IRAF[26] task PSFMATCH (Phillips & Davis 1995). PSF fitting photometry is performed on the subtracted images, and the results from the two routines are averaged whenever appropriate. Artificial stars are injected into the original KAIT images and extracted from the subtracted images to estimate the scatter of

[26] IRAF is distributed by the National Optical Astronomy Observatories, which is operated by the Association of Universities for Research in Astronomy, Inc., under cooperative agreement with the National Science Foundation.

Table 3
Photometry of Comparison Stars in the Field of SN 2008D by KAIT and FLWO 1.2 m

ID	U (mag)	N_U	B (mag)	N_B	V (mag)	N_V	R/r' (mag)	$N_{R/r'}$	I/i' (mag)	$N_{I/i'}$
1	16.771(029)	2	16.438(002)	3	15.563(006)	2	15.117(013)	3	14.640(016)	3
2	17.703(037)	2	17.732(003)	2	16.997(002)	4	16.590(005)	2	16.274(007)	6
3	13.611(005)	3	13.745(008)	3	13.234(010)	4	12.933(010)	4	12.639(015)	3
4	17.822(069)	2	17.865(009)	3	17.409(012)	4	17.061(010)	5	16.781(002)	6
5	...	...	17.994(011)	2	17.316(010)	4	16.841(013)	4	16.498(009)	5
6	...	...	18.132(014)	4	17.550(016)	3	17.115(005)	4	16.856(011)	6
7	12.466(005)	3	12.530(002)	3	...	...	...	...	...	...
8	...	...	18.977(012)	4	17.924(011)	4	17.227(006)	5	16.789(003)	3
9	15.003(007)	3	14.969(003)	3	14.394(016)	3	14.041(010)	3	13.734(013)	3
1	...	...	16.415(049)	1	15.586(033)	1	15.326(045)	1	15.088(046)	1
3	...	...	13.657(031)	1	13.191(022)	1	13.089(031)	1	12.999(031)	1
10	...	...	16.498(049)	1	15.594(033)	1	15.298(045)	1	15.047(045)	1
11	...	...	16.908(051)	1	15.764(035)	1	15.344(047)	1	15.004(048)	1
12	...	...	18.068(089)	1	17.237(060)	1	17.038(079)	1	16.805(081)	1
13	...	...	15.659(040)	1	14.827(027)	1	14.585(037)	1	14.391(037)	1
14	...	...	14.364(033)	1	13.631(023)	1	13.446(031)	1	13.311(031)	1
15	...	...	17.584(086)	1	17.164(058)	1	17.087(076)	1	17.040(078)	1
16	...	...	16.054(045)	1	15.320(031)	1	15.105(041)	1	14.946(042)	1
17	...	...	17.309(055)	1	15.966(037)	1	15.486(049)	1	15.059(051)	1

Notes. Uncertainties (standard deviation of the mean) are indicated in parentheses. Stars (see Figure 3) in the top half of the table were observed with KAIT in *UBVRI* and the stars in the bottom half were observed with the FLWO 1.2 m telescope in $BVr'i'$.

the measurements. To convert the KAIT instrumental magnitudes into the standard Johnson BV and Cousins RI system, the color terms for the KAIT filters as determined from many photometric calibrations are used in the conversion (as detailed by Modjaz et al. 2001 and Li et al. 2001). The final error bars for the magnitudes are the scatter in the artificial-star simulation and the calibration error added in quadrature.

We note that the FLWO 1.2 m telescope template images were taken with the Johnson BV and Sloan $r'i'$ filters, while the KAIT observations of SN 2008D were taken with the Johnson BV and Cousins RI filters. The difference between the $r'i'$ and RI filter transmission curves raises the possibility of a systematic uncertainty during the image-subtraction process. We investigated this issue with the artificial-star simulations and concluded that the systematic uncertainty is smaller than ∼0.03 mag (which is not reported in the final uncertainties).

SN 2008D was remotely observed with the Lick Observatory 1 m Nickel telescope in $BVRI$ on 2008 January 11 and 12. These data were processed with proper bias and flat-field images, and the image subtraction and photometry were performed with the KAIT photometry pipeline (but modified to deal with the Nickel telescope images). The FLWO 1.2 m telescope template images were used to generate the subtracted images, and the Lick calibration and the proper color terms for the Nickel telescope filters are used to convert the instrumental magnitudes into the standard system. The final photometry of SN 2008D from the KAIT and Nickel observations is listed in Table 4.

3.3. FLWO 1.2 m Telescope Data Reduction

The field of SN 2007uy in NGC 2770 was monitored by the FLWO 1.2 m telescope in the context of the CfA SN monitoring[27] efforts when SN 2008D was discovered, providing us with valuable pre-explosion images. We followed SN 2008D on a nightly basis (weather permitting) in $BVr'i'$. For performing photometry of FLWO 1.2 m telescope images, we adopted the image-analysis pipeline of the SuperMACHO and ESSENCE collaborations (see Rest et al. 2005, Garg et al. 2007, and Miknaitis et al. 2007 for details). The operations of this optical photometry pipeline are discussed in depth by Hicken et al. (2009). In brief, we employed differential photometry by measuring the brightness of the SN with respect to a set of stars (see Figure 3) in the SN field and employed the DoPHOT photometry package (Schechter et al. 1993) to measure the flux of the SN and its comparison stars. We performed image subtraction with the robust algorithm of Alard & Lupton (1998; see also Alard 2000), using as templates the 1.2 m images taken on 2008 January 8 of the field. The "FLWO calibration" and the color terms for Keplercam (Modjaz 2007) were used to convert the instrumental magnitudes into the standard system.

We present the 1.2 m FLWO $BVr'i'$ photometry in Table 4. For multiple observations on the same night we report the weighted mean of those observations. Intranight observations did not reveal statistically significant variations for SN 2008D. We furthermore derive upper limits for SN 2008D based on 2008 January 9.44 images of the field of SN 2007uy, three hours before the onset of XRT 080109 (Section 2), and present them in Table 4. The upper limits were estimated by placing fake stars with a range of magnitudes at the position of SN 2008D on the template images and then determining when they are detected at varying thresholds above background.

3.4. UVOT Data Reduction

The *Swift*/UVOT has followed SN 2008D intensively (Kong et al. 2008b; Immler et al. 2008a; Li et al. 2008; Immler et al. 2008b; Soderberg et al. 2008b). We retrieved the level-2 UVOT (Roming et al. 2005) data for SN 2008D from the *Swift* data archive in all available filters (i.e., in the *UVW2*, *UVM2*, *UVW1*, *U*, *B*, and *V* filters).

We used the UVOT observations of SN 2007uy on 2008 January 6 as the template images to reduce the data of SN 2008D (a total exposure time of 808 s in each of the filters). For the *U*, *B*, and *V* filters, we employed the photometric reduction

[27] See http://www.cfa.harvard.edu/supernova/index.html.

Table 4
Optical Photometry of SN 2008D

MJD (day)	Δt[a] (day)	B (mag)	V (mag)	R (mag)	$R(c)$[b] (mag)	r' (mag)	i' (mag)	I (mag)	Tel.[c]
54474.45	−0.12	>20.10	>19.80	···	···	>20.20	> 20.20	···	FLWO
54475.41	0.84	19.08(03)	18.52(04)	···	···	18.31(04)	18.17(03)	···	FLWO
54476.41	1.85	19.05(07)	18.33(04)	17.80(03)	17.78(05)	···	···	17.34(05)	KAIT
54476.43	1.87	18.98(03)	18.38(03)	···	···	18.11(03)	17.86(03)	···	FLWO
54477.35	2.78	19.01(03)	18.39(05)	17.84(03)	···	···	···	17.36(02)	Nickel
54477.36	2.79	19.11(02)	18.44(03)	···	···	18.15(02)	17.86(02)	···	FLWO
54477.46	2.89	19.15(08)	18.43(05)	17.85(04)	17.82(05)	···	–	17.38(04)	KAIT
54478.34	3.78	19.09(03)	18.37(02)	17.89(02)	···	···	···	17.37(02)	Nickel
54478.39	3.83	19.24(02)	18.47(02)	···	···	18.17(02)	17.89(02)	···	FLWO
54478.44	3.87	19.22(09)	18.43(05)	17.83(04)	17.81(05)	···	···	17.40(04)	KAIT
54479.43	4.86	19.14(06)	18.30(04)	17.78(04)	17.76(05)	···	···	17.19(04)	KAIT
54480.39	5.83	19.34(06)	18.22(04)	···	···	18.02(03)	17.72(04)	···	FLWO
54480.40	5.84	19.23(07)	18.22(04)	17.68(03)	17.64(05)	···	···	17.17(03)	KAIT
54481.43	6.86	18.95(11)	17.97(05)	17.47(06)	17.48(05)	···	···	16.97(05)	KAIT
54481.51	6.94	19.10(04)	18.05(04)	···	···	17.75(05)	17.58(09)	···	FLWO
54482.39	7.82	18.88(11)	17.93(05)	17.34(03)	17.31(05)	···	···	16.81(04)	KAIT
54482.43	7.86	18.98(02)	17.94(03)	···	···	17.65(03)	17.34(03)	···	FLWO
54483.27	8.71	18.89(05)	17.70(03)	···	···	17.51(02)	17.25(03)	···	FLWO
54483.36	8.79	18.90(10)	17.73(04)	17.27(02)	17.21(06)	···	···	16.72(03)	KAIT
54484.36	9.79	18.69(07)	17.69(04)	17.13(02)	17.07(06)	···	···	16.58(02)	KAIT
54485.34	10.77	18.54(08)	17.61(05)	17.07(02)	16.97(08)	···	···	16.41(02)	KAIT
54489.41	19.90	18.76(05)	17.63(03)	···	···	17.00(02)	16.87(02)	···	FLWO
54495.36	20.80	18.36(04)	17.38(03)	···	···	17.00(02)	16.65(02)	···	FLWO
54496.34	21.77	18.52(03)	17.41(02)	···	···	16.95(02)	16.59(02)	···	FLWO
54497.39	22.83	18.63(03)	17.40(02)	···	···	17.06(03)	16.68(03)	···	FLWO
54498.30	23.74	18.63(05)	17.50(04)	···	···	17.05(02)	16.65(02)	···	FLWO
54499.35	24.79	18.72(02)	17.49(02)	···	···	17.07(02)	16.70(02)	···	FLWO
54501.42	26.85	18.92(07)	17.54(03)	16.82(02)	···	···	···	16.20(02)	KAIT
54502.36	27.79	19.01(05)	17.58(03)	16.86(02)	···	···	···	16.22(02)	KAIT
54502.44	27.87	18.93(04)	17.51(02)	···	···	17.18(02)	16.77(02)	···	FLWO
54503.34	28.78	19.15(03)	17.67(02)	···	···	17.22(02)	16.78(02)	···	FLWO
54503.38	28.81	19.13(06)	17.64(03)	16.86(02)	···	···	···	16.24(02)	KAIT
54504.35	29.78	19.19(05)	17.74(03)	16.95(02)	···	···	···	16.27(03)	KAIT
54504.37	29.81	19.25(04)	17.71(02)	···	···	17.29(02)	16.83(02)	···	FLWO
54505.33	30.76	19.28(06)	17.82(03)	17.01(02)	···	···	···	16.28(02)	KAIT
54507.32	32.75	19.52(08)	17.92(03)	17.11(02)	···	···	···	16.38(02)	KAIT
54509.29	34.72	19.70(06)	18.06(03)	17.21(02)	···	···	···	16.42(02)	KAIT

Notes. Uncertainties of the measurements are indicated in parentheses.
[a] Time in days since t_0.
[b] $R(c)$-band magnitudes derived from unfiltered observations.
[c] Telescopes used: KAIT = 0.76 m Katzman Automatic Imaging Telescope; Nickel = Lick Observatory 1 m Nickel telescope; FLWO = FLWO 1.2 m telescope.

and calibration as described by Li et al. (2006) to perform photometry of SN 2008D on the subtracted images, while for the Far-UV filters (*UVW2*, *UVM2*, *UVW1*), we used a 3″ aperture and employed the calibration of Poole et al. (2008). Many tests have shown that the two calibrations by Li et al. (2006) and Poole et al. (2008) are consistent with each other.

The UVOT photometry of SN 2008D is reported in Table 5, and is presented in Figure 4, along with the overall optical photometry, with respect to the start of XRT 080109 (Section 2). The UVOT BV values reported here are fully consistent with those in Soderberg et al. (2008b), while our U photometry is systematically fainter by 0.2 mag (consistent within systematic errors, see below), and our *UVW1*, *UVW2*, and *UVM2* 3σ upper limits are systematically fainter by 0.2–1 mag. Our analysis used larger binning periods than that of Soderberg et al., producing deeper images and enabling additional detections in *UVW1*. The S/N of the UV detections is poor, and thus precision photometry is difficult. Specifically, the choice of aperture size affects the

Table 5
Swift/UVOT Photometry of SN 2008D

Δt[a] (day)	δt[b] (day)	Exp[c] (s)	Mag	σ (mag)	Filter
0.1359	0.2688	412.27	20.24	0.21	*U*
2.0047	1.0058	2677.07	18.62	0.03	*U*
2.9769	0.8591	1001.81	19.07	0.06	*U*
3.9479	0.9349	1314.54	19.36	0.07	*U*
4.9872	0.9346	1347.46	19.37	0.07	*U*
5.9550	0.9326	921.90	19.45	0.08	*U*

Notes. Listed uncertainties do not include systematic uncertainties.
[a] Time in days (middle point of the combined image) since t_0 = 2008-01-09 13:32:49.
[b] Time bin in days (from the start of the first exposure to the end of the last exposure in the combined image).
[c] Total exposure time (in seconds).

(This table is available in its entirety in a machine-readable form in the online journal. A portion is shown here for guidance regarding its form and content.)

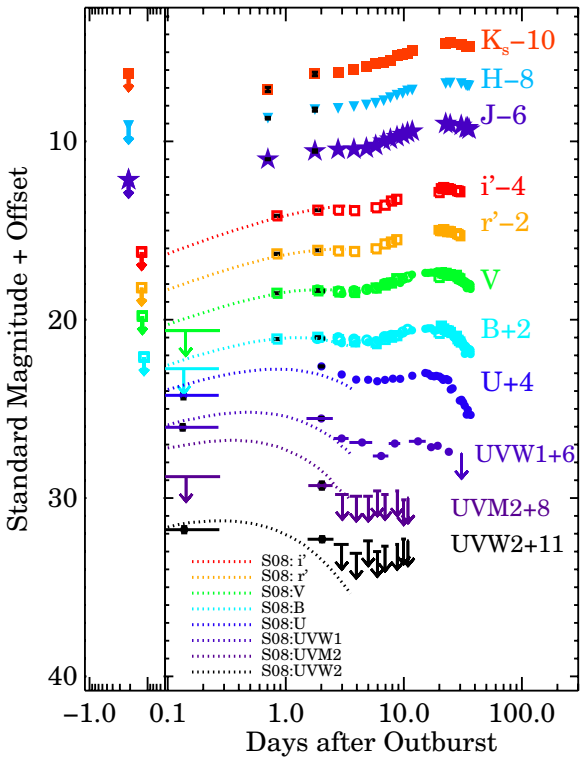

Figure 4. Observed optical and NIR light curves of SN 2008D after the onset (the right panel) of XRT 080109 at t_0 = 2008-01-09 13:32:49 (±5 s), which we adopt as the time of shock breakout. The filled circles show *UVW1*, *UVM2*, *UVW1*, *U*, *B*, *V* data from *Swift*/UVOT, the empty circles are *BV* data from KAIT (its *RI* data are not shown for the sake of clarity), while the empty squares are $BVr'i'$ data from the FLWO 1.2 m telescope. JHK_s data (filled stars, triangles, and squares) are from PAIRITEL. Note the very early optical data points (Δt =0.84 day after shock breakout) from the FLWO 1.2 m telescope, as well as NIR data (at Δt =0.71 day) from PAIRITEL. *Swift*/UVOT upper limits are indicated by the arrows. We also plot the pre-explosion upper limits derived from the 1.2 m CfA (at $\Delta t = -2.8$ hr) and the PAIRITEL (at $\Delta t = -4.5$ hr) data (the left panel). The data have not been corrected for extinction. We note that our earliest ground-based $BVr'i'$ data points are consistent with the light-curve fits by Soderberg et al. (2008, S08; dotted lines), who use the envelope BB emission model from Waxman et al. (2007).

(A color version of this figure is available in the online journal.)

final SN magnitude; for example, using a 2″ aperture for the *UVW1* band gives magnitudes that are ∼0.23 mag brighter than for the 3″ aperture that we adopt (even after appropriate aperture corrections). Thus, we estimate the systematic uncertainty of the final UV photometry to be on the order of ∼0.25 mag.

3.5. Near-Infrared Photometry

We obtained NIR (JHK_s) photometric measurements with the refurbished and fully automated 1.3 m Peters Automated Infrared Telescope (PAIRITEL)[28] located at FLWO. PAIRITEL is the world's largest NIR imaging telescope dedicated to time-domain astronomy (Bloom et al. 2006). The telescope and camera were part of the Two Micron All Sky Survey (2MASS; Skrutskie et al. 2006) project. The *J*-, *H*-, and K_s-band (1.2, 1.6, and 2.2 μm; Cohen et al. 2003) images were acquired simultaneously with the three NICMOS3 arrays with individual exposure times of 7.8 s.

The PAIRITEL reduction pipeline software (Bloom et al. 2006) is used to estimate the sky background from a star-masked median stack of the SN raw images. After sky subtraction, the pipeline is used to cross-correlate, stack, and subsample the processed images in order to produce the final image with an effective scale of 1″pixel^{-1} and an effective field of view (FOV) of 10′×10′. The effective exposure times for the final "mosaic" images ranged from 15 to 20 minutes. Multi-epoch observations over the course of the night (totaling between 40 minutes and 4 hr) were obtained to search for intranight variations, but none were found at a statistically significant level.

For the NIR photometry, we used the image-analysis pipeline of the ESSENCE and SuperMACHO projects (Rest et al. 2005; Garg et al. 2007; Miknaitis et al. 2007). We performed difference photometry (following Wood-Vasey et al. 2008) using the image-subtraction algorithm of Alard & Lupton (1998), similar to our optical photometry. As a template image for the field of SN 2008D, we used our PAIRITEL images of SN 2007uy taken on 2008 January 9. Thus, we also derive NIR upper limits for SN 2008D based on images of the field of SN 2007uy, taken on 2008 January 9 08:26:19, 4.5 hr before t_0, the onset of XRT 080109 (see Section 2), and present them in Table 6. The upper limits were estimated in the same fashion as for the optical data. We performed the final calibration onto the 2MASS system by using as reference stars the field stars from the 2MASS catalog, of which there were 20–30 in the FOV. No color-term corrections were required since our natural system is already in the 2MASS system. We present our PAIRITEL photometry in Table 6.

Table 6
Near-Infrared Photometry of SN 2008D

MJD (day)	Δt (day)	J (mag)	H (mag)	K_s (mag)
54474.35	−0.21	>18.15	>17.12	>16.18
54475.27	0.71	17.00(03)	16.70(05)	17.09(12)
54476.33	1.77	16.54(07)	16.22(09)	16.22(10)
54477.34	2.78	16.45(07)	16.15(09)	16.13(15)
54478.34	3.78	16.44(04)	16.05(09)	15.99(12)
54479.38	4.82	16.38(10)	15.96(10)	15.81(10)
54480.34	5.78	16.23(10)	15.86(10)	15.63(07)
54481.32	6.76	15.99(10)	15.72(07)	15.55(02)
54482.26	7.70	15.88(04)	15.55(00)	15.46(05)
54483.32	8.76	15.74(08)	15.41(13)	15.21(06)
54484.35	9.79	15.62(05)	15.31(05)	15.11(07)
54485.31	10.75	15.51(02)	15.17(16)	15.05(13)
54486.35	11.79	15.43(01)	15.12(05)	14.92(05)
54497.19	22.63	15.00(04)	14.76(08)	14.53(03)
54499.26	24.70	15.07(21)	14.73(03)	14.44(04)
54505.20	30.64	15.11(05)	14.76(02)	14.54(11)
54508.24	33.68	15.25(02)	14.86(01)	14.68(13)
54509.22	34.66	15.24(05)	14.88(03)	14.68(05)
54510.25	35.69	15.32(04)	14.89(06)	14.68(03)

4. EARLY-TIME BROADBAND PHOTOMETRY

Figure 4 shows the UV (*UVW2*, *UVM2*, *UVW1*, *U*), optical ($BVr'i'$), and NIR (JHK_s) photometric evolution of SN 2008D, starting as early as 0.1 day after burst, and going out to 35 days. The data reveal a two-component light curve (Soderberg et al. 2008b): the first due to the cooling stellar envelope that is most expressed in the blue bands ($\Delta t = 0.1$–4 days) and the second due to the standard radioactive decay of ^{56}Ni and ^{56}Co ($\Delta t \gtrsim 5$ days) with half-life times of 6.1 days and 77.3 days, respectively, which lead to energy deposition behind the SN photosphere. A number of theoretical studies have computed shock breakout in the context of SN II 1987A and corresponding optical light

[28] See http://www.pairitel.org/.

curves due to the cooling stellar envelope (e.g., Woosley et al. 1987; Ensman & Burrows 1992; Chevalier 1992; Blinnikov et al. 2000), SN IIb 1993J (e.g., Blinnikov et al. 1998), and broad-lined SN Ic 2006aj (Waxman et al. 2007). In the following, we will concentrate on the models by Waxman et al. (2007) as used by Soderberg et al. (2008b) to fit to the *Swift*/UVOT data and their ground-based data, as well as the most recent model by Chevalier & Fransson (2008). In Section 6.2, we will briefly discuss the implications of the differences between those two models for deriving the progenitor radius.

The most remarkable aspects are the early-time *Swift*/UVOT data and our very early optical and NIR data points (at Δt = 0.84 and 0.71 day, respectively), of which the NIR data are the earliest broadband observations reported of an SN Ib. They were obtained as part of our observing campaign of SN Ib 2007uy in the same galaxy. Here all four ($BVr'i'$) filters indicate a first peak at 0.8–1.8 day. We note that these earliest $BVr'i'$ data points are consistent with the cooling stellar envelope fits (dashed lines in Figure 4) by Soderberg et al. (2008b) to their ground-based data, while the fit in the *UVM2* passband does not agree with the photometry as performed by us; the fit predicts brighter magnitudes than observed, e.g., by ∼0.2 mag for the first *UVM2* upper limit.

Our *V*-band light curve of SN 2008D peaks on 2008 January 27.9 ± 0.5 (i.e., at $\Delta t = 18.3 \pm 0.5$ day) at apparent magnitude $m_V = 17.33 \pm 0.05$ mag. The *B*-band rise time (between shock breakout and maximum light) is slightly shorter than in the *V* band, namely 16.8 ± 0.5 day, peaking on 2008 January 26.4 at $m_B = 18.5 \pm 0.05$ mag. Our apparent peak magnitudes are consistent with other reports within the uncertainties (Soderberg et al. 2008b; Mazzali et al. 2008; Malesani et al. 2009). The rise times of SN 2008D are at the long end of the range of those observed for stripped-envelope SNe, and similar to SN 1999ex (Stritzinger et al. 2002). After correcting for a Galactic extinction and host-galaxy reddening of $E(B-V)_{\rm Host} = 0.6 \pm 0.1$ mag (see Section 6), these values correspond to a peak absolute magnitude of $M_V = -17.0 \pm 0.3$ mag and $M_B = -16.3 \pm 0.4$ mag for SN 2008D, using a distance modulus of $\mu = 32.46 \pm 0.15$ mag (which corresponds to a distance of $D = 31 \pm 2$ Mpc). This distance modulus is based on the measured heliocentric velocity of NGC 2770, corrected for the effect of the Virgo cluster and the Great Attractor by using the local velocity field model given by Mould et al. (2000). These are modest peak luminosities compared to those of other known SNe Ib and SNe Ic, in particular about 1 mag less luminous than the mean of the SN Ib sample in Richardson et al. (2006; $\langle M_V \rangle = -17.9 \pm 1.0$ mag, recomputed using $H_0 = 73$ km s^{-1} Mpc^{-1} for those SN with known luminosity distances), but within the range of observed values. SN 2008D is fainter than SN 1999ex, a well observed SN Ib (by ∼0.5 mag and 0.8 mag in *V* and *B*, respectively) and SN 1993J (by ∼0.4 mag).

5. SPECTROSCOPIC OBSERVATIONS

Optical spectra were obtained with a variety of instruments: Gemini-South via queue-scheduled observations (GS-2007B-Q-2, PI Chen), the 6.5 m MMT, the 10 m Keck I and Keck II telescopes, the 6.5 m Clay Telescope of the Magellan Observatory located at Las Campanas Observatory (LCO), the 3 m Shane telescope at Lick Observatory, the Astrophysical Research Consortium 3.5 m telescope at Apache Point Observatory (APO), and the FLWO 1.5 m telescope. The spectrographs utilized were GMOS-South (Hook et al. 2003) at Gemini, Blue Channel (Schmidt et al. 1989) at the MMT, LRIS (Oke et al. 1995) and HIRES (Vogt et al. 1994) at Keck I, DEIMOS (Faber et al. 2003) at Keck II, LDSS-3 (Mulchaey & Gladders 2005) at LCO, the Kast Double Spectrograph (Miller & Stone 1993) at Lick, the DIS spectrograph at the APO, and the FAST spectrograph (Fabricant et al. 1998) on the FLWO 1.5 m telescope. A detailed journal of observations is shown in Table 7.

Almost all optical spectra were reduced and calibrated employing standard techniques (see, e.g., Modjaz et al. 2001) in IRAF and our own IDL routines for flux calibration. In addition, the HIRES spectrum was reduced using HIRedux,[29] an IDL package developed by one of us (J.X.P.) for the HIRES mosaic, and the GMOS-S and DEIMOS spectra were reduced using slightly different techniques (see Foley et al. 2006, 2007).

Extractions of the low-resolution spectra were done using the optimal weighting algorithm (Horne 1986), and wavelength calibration was accomplished with HeNeAr lamps taken at the position of the targets. Small-scale adjustments derived from night-sky lines in the observed frames were also applied. The spectra were either taken at the parallactic angle (Filippenko 1982), at low airmass, or with an atmospheric dispersion corrector, in order to minimize differential light loss produced by atmospheric dispersion, except for the GMOS-South spectrum. Telluric lines were removed following a procedure similar to that of Wade & Horne (1988) and Matheson et al. (2000b). The final flux calibrations were derived from observations of spectrophotometric standard stars of different colors to correct for second-order light contamination in the MMT and FAST spectrographs (see Modjaz et al. 2008b for more details).

Four NIR spectra were obtained on 2008 January 14.45, 21.51, 28.51 and 2008 March 14.48 using the 3.0 m telescope at the NASA Infrared Telescope Facility (IRTF) with the SpeX medium-resolution spectrograph in prism (LRS) mode (Rayner et al. 2003). The SpeX instrument provides single-exposure coverage of the wavelength region 0.8–2.5 μm in either cross-dispersed or prism mode. The data were reduced and calibrated using a package of IDL routines specifically designed for the reduction of SpeX data (Spextool v3.2; Cushing et al. 2004). Corrections for telluric absorption were performed using the extracted spectrum of an A0V star and a specially designed IDL package developed by Vacca et al. (2003). Additional details of the data acquisition and reduction methods are given by Marion et al. (2009).

5.1. High-resolution Spectroscopy: Probing the Interstellar Medium

We obtained one high-resolution spectrum with Keck I on 2008 January 12.5 (i.e., at $\Delta t = 2.95$ days), over the observed wavelength range 3440–6300 Å. We detect underlying H II region emission lines (Balmer lines and [O II] λ3727) as well as Na I and Ca II H&K absorption lines in the host galaxy (see also Soderberg et al. 2008b; Malesani et al. 2009). The Na I and Ca II H&K absorption lines have identical redshifts as the centroid of the [O II] and Balmer emission lines, $z = 0.00700 \pm 0.00005$. Since both emission and absorption lines show the same velocity, we consider the Na I and Ca II H&K absorption lines to have interstellar origin (as opposed to circumstellar) and attribute the offset of ∼160 km s^{-1} from the measured redshift of the nucleus of the host galaxy NGC 2770 ($z_{\rm nuc} = 0.006451 \pm 0.000087$; Falco et al. 1999) to the galaxy's rotation curve. Given that NGC 2770 is an inclined,

[29] http://www.ucolick.org/∼xavier/HIRedux/index.html

Table 7
Journal of Spectroscopic Observations of SN 2008D

UT Date	Δt[a] (days)	$t_{V\max}$[b] (days)	Telescope[c]	Range[d] (Å)	Airmass[e]	Slit (″)	Exp. (s)
2008 Jan. 11.27	1.70	−16.7	GMOS-S	4000−8500	2.25	0.75	3 ×600
2008 Jan. 11.41	1.84	−16.6	MMT	3200−8400	1.12	1.00	1200
2008 Jan. 12.36	2.80	−15.6	Lick	3300−8100	1.04	2.00	2 × 1200
2008 Jan. 12.55	2.99	−15.4	MMT	3300−8100	1.62	1.00	2 × 300
2008 Jan. 12.67	3.11	−15.3	Keck II	5000−10000	1.64	1.00	300
2008 Jan. 13.30	3.74	−14.7	MMT	3300−8100	1.08	1.00	1200
2008 Jan. 13.38	3.82	−14.6	Lick	3300−8100	1.01	2.00	2 × 1200
2008 Jan. 14.36	4.79	−13.6	MMT	3300−8400	1.00	2.00	1200
2008 Jan. 14.40	4.84	−13.6	Lick	3300−8100	1.01	2.00	4 × 1200
2008 Jan. 14.45	4.89	−13.6	IRTF	8000−25,000	1.07	0.5	10 × 150
2008 Jan. 15.31	5.75	−12.7	MMT	3300−8400	1.05	3.50	1800
2008 Jan. 15.37	5.80	−12.6	Lick	3300−10700	1.02	2.00	2 × 1800
2008 Jan. 16.34	6.77	−11.7	MMT	3300−6500	1.05	1.00	3 × 900
2008 Jan. 18.57	9.00	−9.4	Lick	3500−10700	1.80	2.00	2 × 1800
2008 Jan. 20.27	10.70	−7.7	APO	3500−5600	1.13	1.50	2 × 1200
2008 Jan. 21.22	11.66	−6.8	APO	3300−9800	1.30	1.50	3 × 1200
2008 Jan. 21.51	11.95	−6.5	IRTF	8000−25,000	1.04	0.5	11 × 150
2008 Jan. 28.51	18.95	0.5	IRTF	8000−25,000	1.07	0.5	11 × 150
2008 Feb. 01.35	22.78	4.3	FLWO	3500−7400	1.00	3.00	2 × 1800
2008 Feb. 02.44	23.88	5.4	APO	3300−9800	1.25	1.50	2 × 1200
2008 Feb. 09.12	30.56	12.1	MMT	3300−8400	1.05	1.00	3 × 900
2008 Feb. 11.18	32.61	14.2	MMT	3300−8400	1.05	1.00	3 × 900
2008 Feb. 12.43	33.89	15.4	Keck	3100−9300	1.03	1.00	2 × 900
2008 Feb. 16.36	37.79	19.4	Lick	3300−10700	1.02	2.00	1800
2008 Feb. 27.08	48.52	30.1	LCO	3800−10800	2.57	1.0	3 ×300
2008 Feb. 28.37	49.81	31.4	APO	3300−9800	1.24	1.50	2 × 1200
2008 Mar. 10.23	60.67	42.2	Keck	3100−9100	1.30	1.00	600
2008 Mar. 14.48	63.92	45.5	IRTF	8000−25,000	1.54	0.5	5 × 150
2008 Apr. 28.33	109.77	91.4	Keck	3100−9300	1.30	1.00	2 × 400
2008 Jun. 07.26	149.69	132.4	Keck	3100−9300	1.50	1.00	2 × 900

Notes.
[a] Days after X-ray outburst, t_0 = 2008-01-09 13:32:49 UT.
[b] Days with respect to date of *V*-band maximum.
[c] APO = 3.5 m telescope at Apache Point Observatory/DIS; FLWO = Tillinghast 1.5 m/FAST; GMOS-S = Gemini-South 8.4 m/GMOS; IRTF = IRTF 3 m/SpeX; Keck I = Keck I 10 m/LRIS; Keck II = Keck II 10 m/DEIMOS; LCO = 6.5 m Clay Magellan Telescope at Las Campanas Observatory/LDSS-3; Lick = Lick 3 m/Tillinghast; MMT = 6.5 m MMT/Bluechannel.
[d] Airmass at the middle of the set of observations.
[e] Observed wavelength range of spectrum. In some cases, the blue and red ends of the spectrum are extremely noisy and are not shown in the figures.

edge-on, typical spiral (Sb/Sc) galaxy (Soderberg et al. 2008b; Thöne et al. 2009), rotation on the order of 160 km s^{-1} at the distance of the SN from the nucleus (∼9 kpc) is plausible; the full rotation curve of NGC 2770 extends to ∼400 km s^{-1} (Haynes et al. 1997).

Since the absorption lines are saturated, we can only place lower limits to the column densities of Na I and Ca II H&K: $N_{\rm Na\,I} > 1.0 \times 10^{13}$ cm^{-2} and $N_{\rm Ca\,II} > 1.4 \times 10^{13}$ cm^{-2}. We measure an equivalent width (EW) for Na I D$_2$ of 0.67 ± 0.04 Å (at rest) and for Ca II K of 0.55 ± 0.04 Å (at rest).

5.2. Low-resolution Spectroscopy

In Figure 5, we present the sequence of early-time optical spectra after subtracting the SN recession velocity, dereddened by $E(B-V)_{\rm Host} = 0.6 \pm 0.1$ mag (Section 6). Furthermore, the spectra are labeled according to age (Δt) with respect to date of shock breakout (t_0 = 2008-01-09 13:32:49) and epoch ($t_{V\max}$), defined as days relative to *V*-band maximum (2008 January 27.9 = JD 2454493.4, see Section 4). Knowing both reference dates is crucial for interpreting the spectra and their temporal evolution.

These are amongst the earliest spectra presented of a normal SN Ib (starting 1.70 day after shock breakout, which means 17.0 days before *V*-band maximum) and provide insights into the different layers of the SN ejecta. As the photosphere recedes with time, it reveals lower-velocity material since the SN ejecta are in homologous expansion (where $v \propto R$). Moreover, we obtained late-time spectra at $t_{V\max}$ = +91 and +132 days that show the advent of the nebular epoch, in which the spectrum is marked by strong forbidden emission lines of intermediate-mass elements [O I] and [Ca II] (not shown in Figure 5). We discuss the late-time spectra in Section 8.

At early times, our densely time-sampled series shows the dereddened spectra to consist of a blue, nearly featureless continuum (except around 4000 Å), with superimposed characteristic broad SN lines not attributed to hydrogen (Malesani et al. 2008; Blondin et al. 2008a; Valenti et al. 2008b; Soderberg et al. 2008b). In Section 5.3, we discuss the fleeting, double-

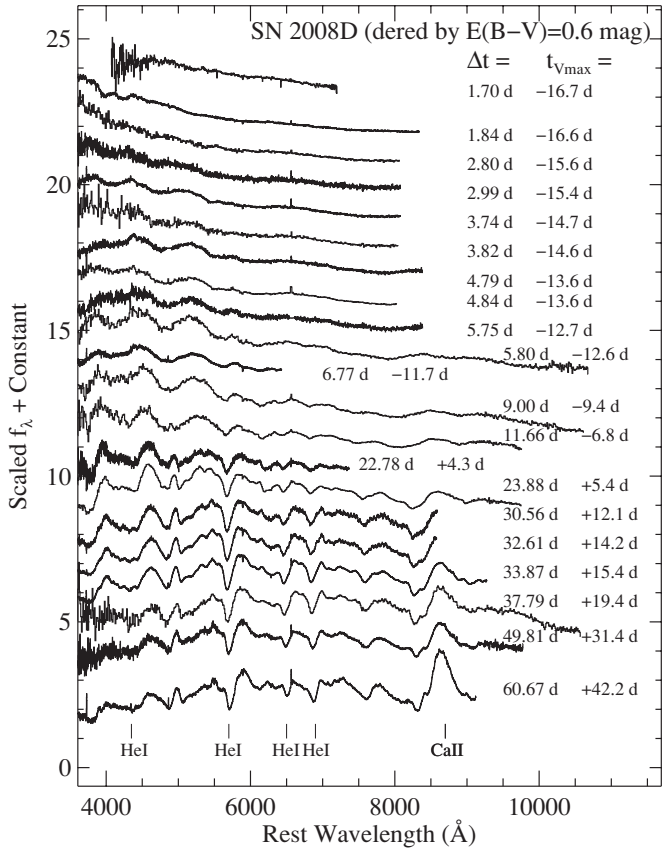

Figure 5. Spectral evolution of SN 2008D, dereddened by $E(B-V)_{\rm Host} = 0.6$ mag and labeled with respect to date of shock breakout, t_0 = 2008-01-09 13:32:49 (indicated by Δt), and to date of V-band maximum, 2008 January 27.9 (indicated by $t_{V\rm max}$). Note the fleeting double-absorption feature around 4000 Å in our early spectrum at $\Delta t = 1.84$ day, which is discussed in Section 5.3. Some spectra have been binned to more clearly visualize their effective S/N. Unfortunately, we have a gap in our spectroscopic coverage around maximum light. The characteristic optical He I lines (due to blueshifted He I λλ4471, 5876, 6678, 7061) become visible starting $\Delta t \approx 12$ days or $t_{V\rm max} \approx -6$ days. Note that not all spectra are presented in this figure. For late-time spectra, see Section 8.

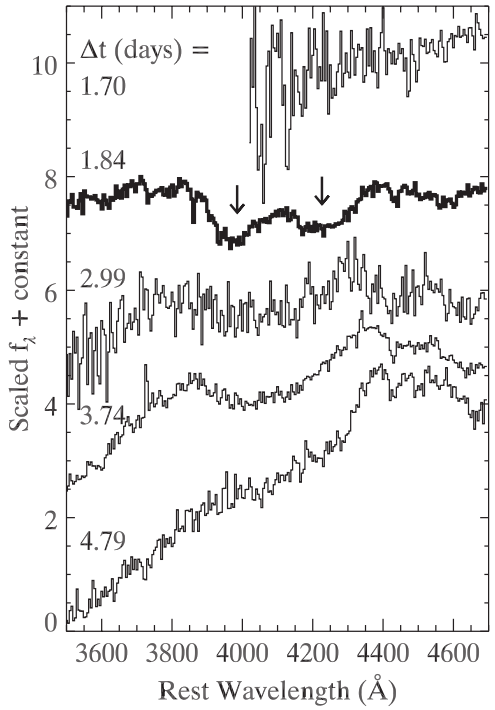

Figure 6. Early-time spectra of SN 2008D in the range 3500–4700 Å, from $\Delta t = 1.70$ to $\Delta t = 4.79$ days past the X-ray outburst, not corrected for reddening. The transient double-absorption feature is marked with arrows in the spectrum at $\Delta t = 1.84$ day.

absorption feature around 4000 Å, which is only seen in our spectrum at $\Delta t = 1.84$ days.

Figure 5 shows that the optical helium lines (blueshifted He I λλ4471, 5876, 6678, 7061) become apparent starting at $\Delta t \approx 10$–12 days (8–6 days before V-band maximum) and grow stronger over time, allowing this SN to be classified as an SN Ib (Modjaz et al. 2008a; Valenti et al. 2008a; see also Soderberg et al. 2008b; Mazzali et al. 2008; Malesani et al. 2009). This is in stark contrast to all SNe associated with GRBs that have been exclusively broad-lined SN Ic (e.g., Galama et al. 1998; Stanek et al. 2003; Hjorth et al. 2003; Malesani et al. 2004; Modjaz et al. 2006; Mirabal et al. 2006; Campana et al. 2006; Pian et al. 2006).

5.3. The Double-absorption Feature Around 4000 Å

Perhaps the most intriguing aspect of the very early time spectra of SN 2008D is the transient, prominent, double-absorption feature around 4000 Å (Figure 6). It is only present in our second spectrum, the MMT+Blue Channel spectrum taken on January 11.41 ($\Delta t = 1.84$ day), and was first noted by Blondin et al. (2008a).

Furthermore, Malesani et al. (2009) obtained spectra of SN 2008D at nearly the same epoch, January 11.32 (i.e., within two hours of our Gemini and MMT spectra, see Table 7) with wavelength range extending down to 3700 Å, and note that their spectra show the same double-absorption feature. The double-absorption feature is apparently absent from our very first spectrum, the Gemini+GMOS spectrum taken on January 11.26, but the spectrum is extremely noisy below ∼4500 Å due to the particular setup used. The spectrum of Soderberg et al. (2008b) on the same and subsequent nights apparently does not extend sufficiently far to the blue to include this feature at ∼4000 Å (their Figure 3). The double-absorption line is no longer visible in spectra taken $\gtrsim 1$ day later (i.e., $\Delta t \gtrsim 2.99$ days) and the two components appear to blend into a single, broad (FWHM ≈23,000 km s^{-1}) absorption feature (maximum absorption at rest frame ∼4100 Å), as clearly seen in the January 13.30 MMT+Blue Channel spectrum ($\Delta t = 3.74$ days) in Figure 6. Also, spectra taken by Malesani et al. (2009) do not show the feature in spectra taken after January 13.07, i.e., $\Delta t \gtrsim 3.51$ days.

The double-absorption feature appears to consist of two overlapping P-Cygni profiles, with rest-frame full width at half-maximum (FWHM) of ∼11,500 km s^{-1} and ∼11,000 km s^{-1} for the bluer (maximum absorption at rest-frame wavelength ∼3980 Å) and redder (maximum absorption at rest-frame wavelength ∼4240 Å) absorptions, respectively. Both absorption components are thus significantly narrower than other absorption features in the same spectrum, whose FWHM ranges between ∼15,000 km s^{-1} and ∼30,000 km s^{-1}.

In the following section we attempt to address the line identification for this feature. Amongst the published supernova spectra, the closest match to the "W" feature that we can find is in the earliest spectrum of SN 2005ap (Quimby et al. 2007) from 2005 March 7 (∼1 week before maximum light), which shows a similar feature at slightly redder wavelengths (by ∼200 Å). Quimby et al. used the parameterized supernova spectrum synthesis code SYNOW (Fisher et al. 1999; Branch

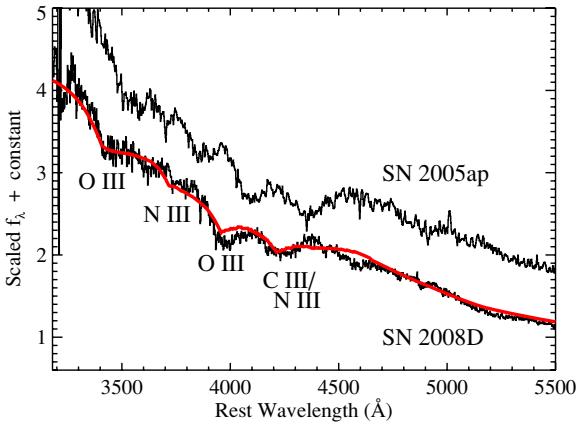

Figure 7. Reddening-corrected early-time spectrum of SN 2008D (black) at $\Delta t = 1.84$ day (2008 January 11.41) and for comparison, the spectrum of SN 2005ap (Quimby et al. 2007). The fit via the parameterized spectral synthesis code SYNOW is shown in red: the "W," along with some other weaker features, can be reproduced with a combination of O III and C III/N III.

(A color version of this figure is available in the online journal.)

et al. 2002) to fit that spectrum with four ions. They ascribed the "W" feature to a combination of C III, N III, and O III with a photospheric velocity of 21,000 km s^{-1}. We downloaded the spectrum of SN 2005ap from the SUSPECT database,[30] generated SYNOW models using only those three ions, and were able to satisfactorily reproduce the "W" feature in SN 2005ap using similar fitting parameters to those of Quimby et al. We then increased what SYNOW calls the "photospheric velocity" ($v_{\rm phot}$) of the fit to match the observed wavelengths of the "W" feature in SN 2008D and found that $v_{\rm phot} \approx 30{,}000$ km s^{-1} produced a good match to the "W" as well as to some other weaker features, as shown in Figure 7 (using a continuum temperature of ∼13,000 K, consistent with the BB temperature as derived from our photometry data, Table 8). SYNOW did not produce any other strong features that are associated with these ions, matching the full extent of the observed MMT spectrum.

While our SYNOW fit produces a good match to the data, we note that SYNOW fits do not produce unique line identifications and the suggested identification here needs to be confirmed by detailed spectral modeling (Mazzali & Lucy 1998; Baron et al. 1999; Dessart & Hillier 2008). Furthermore, while the "W" feature is no longer visible in spectra of SN 2008D taken ∼1 day later (see also Malesani et al. 2009), it seemed to linger for ∼1 week in the spectrum of SN 2005ap (at slightly lower velocities).

At face value, an identification of the "W" feature with C III, N III, and O III at high velocities seems plausible. We expect the early supernova spectrum to have high velocities based on an extrapolation of the observed velocities at late times back to the earliest observations. In addition, what SYNOW designates as the "excitation temperature" is high ($T_{\rm ex} \approx 17{,}000$ K) at these early times[31] and many of the elements that will contribute to the later spectra are more highly ionized. The transient nature of the feature might then be explainable because the elements involved will recombine to lower ionization stages as the ejecta cool (at ∼15,000 K where most of doubly ionized elements recombine to singly ionized species).

Alternatively, the reason for the short-lived nature of this "W" feature could be asphericity in the SN ejecta. We have evidence from late-time spectra for asphericity in at least the inner SN core (see Section 8), which may be connected to some inhomogeneity in the SN ejecta density or chemical abundance profile at the outermost radii that the early-time spectra are probing. If indeed asphericity is involved, then existing spectral synthesis codes (such as SYNOW which assumes spherical symmetry) are challenged to accommodate that aspect.[32]

Table 8
Blackbody Fits and Bolometric Light Curves of SN 2008D from *UVW1* → K_s Data

Δt (days)	$T_{\rm BB}$ (K)	$R_{\rm BB}$ (10^{14} cm)	$\log(L_{\rm BB})$ (erg s^{-1})	$\log(L_{UVW1-K_s})$ (erg s^{-1})
0.80	12000^{+3000}_{-2000}	$2.75^{+0.36}_{-0.37}$	$42.04^{+0.27}_{-0.21}$	$41.92^{+0.18}_{-0.17}$
1.80	10000^{+1600}_{-1200}	$3.78^{+0.30}_{-0.30}$	$42.05^{+0.19}_{-0.17}$	$42.00^{+0.17}_{-0.16}$
2.80	8700^{+1300}_{-1000}	$4.64^{+0.47}_{-0.46}$	$41.93^{+0.17}_{-0.15}$	$41.89^{+0.15}_{-0.14}$
3.80	7900^{+1000}_{-830}	$5.19^{+0.47}_{-0.47}$	$41.86^{+0.15}_{-0.13}$	$41.83^{+0.14}_{-0.13}$
4.80	7600^{+970}_{-780}	$5.62^{+0.52}_{-0.50}$	$41.87^{+0.14}_{-0.13}$	$41.85^{+0.14}_{-0.12}$
5.80	7400^{+910}_{-740}	$6.12^{+0.56}_{-0.54}$	$41.90^{+0.14}_{-0.12}$	$41.89^{+0.13}_{-0.12}$
6.80	7200^{+850}_{-690}	$6.92^{+0.61}_{-0.60}$	$41.95^{+0.13}_{-0.12}$	$41.93^{+0.13}_{-0.12}$
7.80	7000^{+800}_{-660}	$7.64^{+0.65}_{-0.64}$	$42.00^{+0.13}_{-0.11}$	$41.98^{+0.13}_{-0.12}$
8.80	6900^{+770}_{-630}	$8.30^{+0.69}_{-0.69}$	$42.04^{+0.13}_{-0.11}$	$42.02^{+0.12}_{-0.11}$
9.80	6800^{+740}_{-610}	$8.89^{+0.74}_{-0.73}$	$42.08^{+0.12}_{-0.11}$	$42.05^{+0.12}_{-0.11}$
10.80	6700^{+720}_{-590}	$9.45^{+0.78}_{-0.76}$	$42.10^{+0.12}_{-0.11}$	$42.08^{+0.12}_{-0.11}$
11.80	6600^{+700}_{-580}	$9.95^{+0.79}_{-0.81}$	$42.13^{+0.12}_{-0.11}$	$42.11^{+0.12}_{-0.11}$
12.80	6600^{+680}_{-570}	$10.40^{+0.84}_{-0.83}$	$42.15^{+0.12}_{-0.10}$	$42.13^{+0.12}_{-0.11}$
13.80	6500^{+660}_{-550}	$10.80^{+0.92}_{-0.84}$	$42.17^{+0.11}_{-0.10}$	$42.15^{+0.12}_{-0.11}$
14.80	6400^{+650}_{-540}	$11.20^{+0.94}_{-0.86}$	$42.18^{+0.11}_{-0.10}$	$42.17^{+0.12}_{-0.11}$
15.80	6400^{+630}_{-530}	$11.60^{+0.90}_{-0.93}$	$42.19^{+0.11}_{-0.10}$	$42.18^{+0.12}_{-0.11}$
16.80	6300^{+620}_{-520}	$11.90^{+0.97}_{-0.89}$	$42.20^{+0.11}_{-0.10}$	$42.19^{+0.11}_{-0.11}$
17.80	6200^{+600}_{-510}	$12.30^{+0.98}_{-0.96}$	$42.21^{+0.11}_{-0.10}$	$42.20^{+0.11}_{-0.10}$
18.80	6200^{+590}_{-500}	$12.60^{+1.00}_{-0.97}$	$42.21^{+0.11}_{-0.10}$	$42.20^{+0.11}_{-0.10}$
19.80	6100^{+570}_{-480}	$12.90^{+1.00}_{-0.98}$	$42.21^{+0.11}_{-0.10}$	$42.20^{+0.11}_{-0.10}$
20.80	6000^{+560}_{-470}	$13.20^{+1.00}_{-0.99}$	$42.21^{+0.10}_{-0.10}$	$42.20^{+0.11}_{-0.10}$
21.80	6000^{+540}_{-460}	$13.40^{+1.10}_{-1.00}$	$42.20^{+0.10}_{-0.09}$	$42.20^{+0.11}_{-0.10}$
22.80	5900^{+530}_{-450}	$13.70^{+1.00}_{-1.00}$	$42.19^{+0.10}_{-0.09}$	$42.19^{+0.11}_{-0.10}$
23.80	5800^{+520}_{-440}	$13.90^{+1.10}_{-1.00}$	$42.18^{+0.10}_{-0.09}$	$42.18^{+0.10}_{-0.10}$
24.80	5700^{+500}_{-430}	$14.20^{+1.10}_{-1.10}$	$42.17^{+0.10}_{-0.09}$	$42.16^{+0.10}_{-0.10}$
25.80	5600^{+480}_{-410}	$14.50^{+1.10}_{-1.10}$	$42.15^{+0.09}_{-0.09}$	$42.15^{+0.10}_{-0.09}$
26.80	5400^{+460}_{-400}	$14.80^{+1.20}_{-1.10}$	$42.13^{+0.09}_{-0.08}$	$42.13^{+0.10}_{-0.09}$
27.80	5300^{+440}_{-380}	$15.20^{+1.20}_{-1.20}$	$42.11^{+0.09}_{-0.08}$	$42.11^{+0.10}_{-0.09}$
28.80	5200^{+420}_{-360}	$15.50^{+1.20}_{-1.20}$	$42.09^{+0.09}_{-0.08}$	$42.09^{+0.10}_{-0.09}$
29.80	5100^{+400}_{-350}	$15.70^{+1.20}_{-1.20}$	$42.08^{+0.09}_{-0.08}$	$42.08^{+0.10}_{-0.09}$
30.80	5100^{+400}_{-350}	$15.80^{+1.20}_{-1.20}$	$42.06^{+0.08}_{-0.07}$	$42.07^{+0.09}_{-0.09}$

Notes. Adopted values: $E(B-V)_{\rm Host} = 0.6 \pm 0.1$ mag, $D = 31 \pm 2$ Mpc, and $t_0 = 2008\text{-}01\text{-}09\ 13{:}32{:}49$ UT. The uncertainties include the uncertainty in reddening, but not the systematic uncertainty in distance.

6. BOLOMETRIC LIGHT CURVES

Many lines of evidence indicate significant host-galaxy extinction toward SN 2008D: the high-resolution spectrum (Section 5.1) shows strong interstellar Na I D and Ca II lines at the recession velocity of the host galaxy (with EW[Na I D] = 0.7 Å), while low-resolution spectra show in addition diffuse interstellar bands (Herbig 1975). From Soderberg et al. (2008b), we adopt $E(B-V)_{\rm Host} = 0.6$ mag for SN 2008D, and a Milky

[30] http://bruford.nhn.ou.edu/ suspect/index1.html

[31] The apparent incongruence between the excitation and continuum temperatures probably arises from the LTE (local thermodynamic equilibrium) assumption in the SYNOW code (Branch et al. 2002), or because we underestimated the reddening, but this is less likely.

[32] The MMT spectra (including the one displaying the double-absorption feature) will be made publicly available through the CfA Supernova Archive at http://www.cfa.harvard.edu/supernova/SNarchive.html.

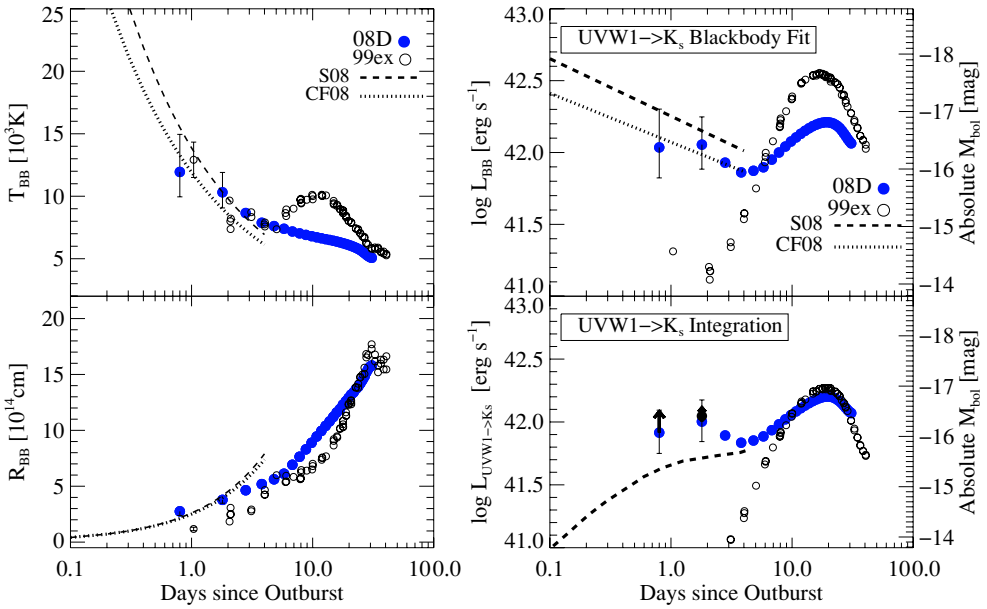

Figure 8. Left: temperature (top) and radius (bottom) derived from a BB fit to the optical and NIR SED of XRT 080109/SN 2008D (filled circles) as a function of time, assuming $D = 31 \pm 2$ Mpc and corrected for reddening ($E(B-V)_{\rm Host} = 0.6 \pm 0.1$ mag). The error bars include the uncertainties as reported from the formal fits, as well as the effect of uncertain extinction. SN 1999ex (open circles, Stritzinger et al. 2002) is shown for comparison. We compare our SN 2008D data to the values of the stellar cooling envelope model (dashed lines) in Soderberg et al. (2008, S08), using the same parameters (in particular, $R_\star \approx R_\odot$) as well as to the model of Chevalier & Fransson (2008, CF08, with their suggested $R_\star \approx 9\ R_\odot$). Right: bolometric light curves of XRT 080109/SN 2008D (filled circles) computed via two different techniques: fitting a BB to the reddening-corrected *UVW1* → K_s fluxes ($L_{\rm BB}$, top) and via direct integration of the reddening-corrected broadband photometry ($L_{UVW1 \rightarrow K_s}$, bottom). The black data point at 1.8 days includes the detections in the Far-UV filters and thus represents $L_{UVW2 \rightarrow K_s}$. We note that the value for the bolometric magnitude $M_{\rm bol}$ of SN 2008D will vary depending on the passband used over which different authors (S08; Malesani et al. 2009) integrate its flux. (A color version of this figure is available in the online journal.)

Way extinction law (Fitzpatrick 1999) with $R_V = 3.1$. This value is used to deredden all of our spectra and is consistent with the value adopted by Mazzali et al. (2008), but 0.2 mag smaller than that used by Malesani et al. (2009). The choice of extinction law does not strongly affect our results.

This value for the reddening is consistent with fitting an absorbed BB spectrum to the spectral energy distribution (SED) of SN 2008D constructed from our simultaneous broadband (*UVW2* → K_s) photometry (see Section 6.1).

In addition, the comparison of spectra and $B-V$ colors of SN 2008D with those of other SNe Ib at comparable epochs, such as SN 1999ex (Stritzinger et al. 2002; Hamuy et al. 2002), yields $E(B-V) = 0.6$–0.7 mag. In particular, we compared SN 2008D with SN 2005hg, a normal SN Ib that suffered very little host-galaxy extinction (Modjaz 2007). Comparison of the spectra (Section 7.2) and the broadband SEDs constructed from our $UBVr'i'JHK_s$ photometry for both SNe indicates a host-galaxy extinction for SN 2008D of $E(B-V) \approx 0.65$ mag, if both SNe have similar color evolution.

6.1. Constructing Bolometric Light Curves

The broadband data set (spanning 2200–24,100 Å) presented here lends itself uniquely to computing the bolometric output of SN 2008D. We determine it in two different ways: (a) by fitting a BB to the broadband photometry and deriving the equivalent BB luminosity ($L_{\rm BB}$) by analytically computing the corresponding Planck function, and (b) by performing a direct integration of the $UVW1BVRr'Ii'JHK_S$ broadband magnitudes ($L_{UVW1 \rightarrow K_s}$), including the far-UV filters *UVW2* and *UVM2* in case of detections. In both cases, the *Swift* UV and our NIR data are crucial, as they provide a factor of at least two in wavelength coverage and leverage for the SEDs. While theoretical considerations might justify using a simple BB approximation for the SN emission shortly after shock breakout (Waxman et al. 2007; Chevalier & Fransson 2008), we do note that without detailed models of SN Ib/c atmospheres, it proves difficult to say how well BB fits approximate the true SN luminosity over the full light curve of SN 2008D. We address this question more in the remainder of the section, when comparing the bolometric luminosities computed via BB fits and those via direct integration.

We start by interpolating the light curves by *Swift*/UVOT (in *UVW1*, *UBV*), FLW0 1.2 m (in $r'i'$), and PAIRITEL (in JHK_s) onto a grid spaced regularly in time, as the observing times were different for different telescopes. We then sampled those light curves at intervals closest to the actual observing time of *Swift*/UVOT and the FLWO telescopes. After removing extinction ($E(B-V)_{\rm Host} = 0.6 \pm 0.1$ mag and assuming a Milky Way extinction law parameterization with $R_V = 3.1$; Fitzpatrick 1999), we converted our photometry into monochromatic fluxes at the effective wavelengths of the broadband filters, using zero points from Fukugita et al. (1995; for $UBVr'i'$, since the UVOT *UBV* photometric system is close to the Johnson *UBV* with Vega defining the zero point; Poole et al. 2008) and Cohen et al. (2003) (for JHK_s). We included 0.05 mag of systematic error in the UVOT filters (Li et al. 2006) and 4% conversion error when using Fukugita et al. (1995).

For our first method, we perform a least-squares fit of a BB spectrum to the SED of each epoch and constrain the derived BB temperature ($T_{\rm BB}$), BB radius ($R_{\rm BB}$), and BB luminosity ($L_{\rm BB}$) as a function of age (see Table 8 and Figure 8). The error bars include the uncertainties from the formal fits as well as uncertainties introduced by the uncertain reddening (± 0.1 mag), which affect the derived BB fit parameters differently, depending on the underlying SED.

We do not include the systematic uncertainty in distance (of order ∼20%). At later times ($\Delta t \gtrsim 8$–10 days) the assumption of a BB continuum is expected to break down, based on the optical spectra where distinct absorption lines develop (see Figure 5). While the χ^2 values of the fits are strictly not acceptable except at early times (1 day $< \Delta t <$ 5 days), the overall fits are reasonable even beyond this time with no obvious residual trends, and we consider the BB measured temperatures, radii, and luminosities still to be generally quite reliable. Thus, the UVOPTIR data are well fit by a BB, especially at early times (and $\Delta t <$ 5 days), and we do not detect any NIR excess (e.g., due to potential dust formation). For clarification, we note that the optical/NIR data to which we fit a BB were obtained much later ($\Delta t \gtrsim 10^5$ s) than when the main X-ray emission period of XRT 080109 occurred ($\Delta t \lesssim 10^3$ s, Section 2). For $\Delta t = 1.8$ days, we detect the SN in the *Swift UVW2* and *UVM2* band and include those data in the BB fit, though their inclusion does not have a significant effect on the outcome (the parameters change by less than 2%).

We present the resultant BB luminosity evolution in Figure 8 (right, the top panel) and include that of SN 1999ex for comparison (from Table 8 of Stritzinger et al. 2002, for their adopted values of $E(B-V) = 0.28$ mag, and explosion date of JD 2,451,480.5), but with a luminosity distance recomputed with $H_0 = 73$ km s^{-1} Mpc^{-1}. Both SNe exhibit the initial dip from the cooling stellar envelope emission, with SN 2008D showing a much less pronounced contrast between dip and peak due to heating of ^{56}Ni than in SN 1999ex.

The second method for computing the bolometric light output is by direct integration of the observed broadband photometry. Here we are in the favorable position of having NIR data, as the NIR contribution to the bolometric output is usually unknown for SNe Ib/c and can be quite large (30%–50%) for certain SNe at late time (>20 days; Tominaga et al. 2005; Tomita et al. 2006; Modjaz 2007), and even larger for dust-producing SNe (SN 2006jc, e.g., Smith et al. 2008; Di Carlo et al. 2008; Modjaz 2007).

We integrate the total optical and NIR monochromatic fluxes in the region between the effective wavelengths of the *UVW1* and K_s filters via the trapezoid approximation. For this purpose, we extrapolate the SED to zero at the blue *UVW1* (2220 Å) and red K_s (24,210 Å) edges of the total set of filters. We plot the resultant bolometric light curve ($L_{UVW1\rightarrow K_s}$) in Figure 8 (right, the bottom panel) and, for comparison, also that of SN 1999ex (based on $U \rightarrow z$ integration; Stritzinger et al. 2002).

For SN 2008D, we find that the bolometric luminosity based on direct *UVW1* $\rightarrow$ K_s integration is very similar to that based on the BB fits (within $\lesssim 0.04$ dex or $\lesssim 8\%$), except for the first three data points at $\Delta t = 0.8$, 1.8, and 2.8 days (different by a factor 1.32, 1.13, and 1.09, respectively). SN 2008D reaches bolometric peak at $\Delta t = 19.2 \pm 0.3$ days with a bolometric peak luminosity of $\log L_{\rm bol} = 42.2 \pm 0.1$ erg s^{-1}, i.e., $M_{\rm bol} = -16.8 \pm 0.1$ mag.

At $\Delta t = 0.84$ day, the peak of the SED is at wavelengths bluer than the observed wavelength coverage and explains the missing flux in the direct integration, which is the absolute lower limit to the total light output. We note that for SN 2008D, the agreement between bolometric values derived from BB fits and those based on direct integration is much better than for SN 1999ex; if the emission from SN 1999ex can be as well described by a BB as that of SN 2008D, then the true bolometric peak luminosity of SN 1999ex is not −17.0 mag (Figure 8), but rather −17.7 mag; i.e., the SN is more luminous than previously thought, because it was not observed in the UV nor in the NIR whose data could have been used to construct a full bolometric output.

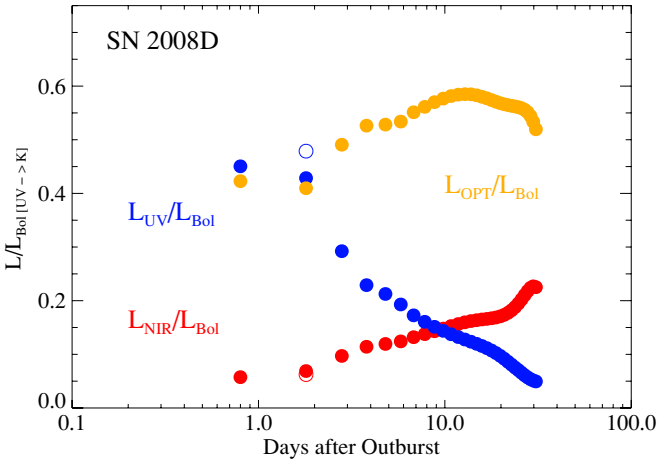

Figure 9. Contribution of the UV (*UVW1*, *U*: blue circles), optical ($BVr'i'$: orange circles), and NIR (JHK_s: red circles) passbands to the bolometric luminosity $L_{\rm int}$ as a function of age for SN 2008D. The empty circles at 1.8 day denote the contributions when including the Far-UV detections (in the *UVM2*, *UVW2* filters).

(A color version of this figure is available in the online journal.)

In Figure 9, we present the contribution of different passbands to the full bolometric luminosity output $L_{UVW1\rightarrow K_s}$ as a function of SN age. At early times, the UV is 40% of the bolometric luminosity. At later times (30 days after outburst), the NIR is 20%. Most supernova observations lack these measurements, so their derived bolometric flux has significant uncertainties.

6.2. Constraining the Progenitor Size of XRT 080109/SN 2008D

Now we compare our data to the fits of Soderberg et al. (2008b) via the cooling BB envelope model of Waxman et al. (2007), and to the predictions of Chevalier & Fransson (2008) as the source for the early-time emission, where the stellar envelope expands and cools after the passage and breakout of the shock wave.

In both models, the time evolution of the radius and the temperature of the cooling envelope are weak functions of the ejecta mass ($M_{\rm ej}$) and ejecta kinetic energy ($E_{\rm K}$), and a stronger function of the radius of the progenitor before explosion ($R_\star$) to the power of 1/4. Both models assume that the photophere is in the outer shock-accelerated part of the SN ejecta density profile, but their methods differ. In the following, we use our early-time light-curve data to provide constraints on $R_\star$ if the ratio $E_{\rm K}/M_{\rm ej}$ can be measured independently from the SN light curves and spectra (Soderberg et al. 2008b; Mazzali et al. 2008; Tanaka et al. 2009).

Analytically, we can rewrite the equations for the radius and the temperature of the cooling envelope as given by W07 and CF08 (Equations (18) and (19), and Equations (2) and (5), respectively), and generalize such that

$$\frac{R_\star}{10^{11}\,{\rm cm}} = C\,T_{\rm BB,ev}^4\,R_{\rm BB,14}^{0.4}\,\Delta t_{\rm d}^{\alpha}\left(\frac{E_{\rm K,51}}{M_{\rm ej,\odot}}\right)^{\beta}, \qquad (1)$$

with

$$C = 0.286 \ \text{for W07 or} \ 3.028 \ \text{for CF08},$$
$$\alpha = 1.69 \ \text{for W07 or} \ 1.61 \ \text{for CF08},$$
$$\beta = -0.24 \ \text{for W07 or} \ -0.27 \ \text{for CF08},$$

where $T_{\rm BB,ev}$ is the BB temperature of the photosphere in eV, $R_{\rm BB} = 10^{14} R_{\rm BB,14}$ cm, $\Delta t_{\rm d}$ time in days after shock breakout, $E_{\rm K} = 10^{51} E_{\rm K,51}$ erg, and $M_{\rm ej} = M_{\rm ej,\odot}\ M_\odot$. Thus, the derived BB fits to the early-time data yield independent measurements of $R_\star$ for each epoch, for a given $E_{\rm K}/M_{\rm ej}$, whose uncertainty does not influence the value of $R_\star$ significantly, given the very weak dependence of $R_\star$ on $E_{\rm K}/M_{\rm ej}$. While the power-law scalings of the parameters are fairly similar for the two models, their largest discrepancy lies in a factor of ∼10 difference in the constant C, which is primarily caused by the factor of ∼2 difference in the temperature equations, as noted by CF08, and by the high sensitivity of $R_\star$ on $T_{\rm BB}$.

Here we explicitly calculate $R_\star$ for the two models with our own data combined with published values of $E_{\rm K}/M_{\rm ej}$ and include all relevant sources of uncertainties; using the slightly different values for $E_{\rm K}/M_{\rm ej}$ for SN 2008D from the literature (Soderberg et al. 2008b; Mazzali et al. 2008; Tanaka et al. 2009), and our estimates for $T_{\rm BB}$ and $R_{\rm BB}$ (Table 8), we compute $R_\star$ for each of the first four epochs ($0.8 < \Delta t < 3.8$ days), and for the range of adopted extinction values ($E(B-V)_{\rm Host} = 0.6 \pm 0.1$ mag). Taking an average over the epochs and using the different reddening values as bounds, we obtain for the W07 model $R_\star^{\rm W07} = (8.6 \pm \sigma_{\rm Ex} + \sigma_{\rm E/M}) \times 10^{10}$ cm, where $\sigma_{\rm Ex}$ and $\sigma_{\rm E/M}$ refer to the systematic error due to uncertain extinction and uncertain $E_{\rm K}/M_{\rm ej}$, respectively, with $\sigma_{\rm Ex} = 4.8$ and $\sigma_{\rm E/M} = 0.4$. In other words, $R_\star^{W07} = 1.2 \pm 0.7 \pm 0.06\ R_\odot$. Likewise for the CF08 model, $R_\star^{\rm CF08} = (86 \pm 45 \pm 4) \times 10^{10}\ {\rm cm} = 12 \pm 7 \pm 0.6\ R_\odot$. Thus, $R_\star$ as derived from the cooling stellar envelope emission is 10 times larger according to the CF08 model than according to the W07 model. CF08 had noted this fact, and furthermore, that their larger progenitor size is consistent with $R_\star^{\rm X-ray} \approx 9\ R_\odot$ based on their simple interpretation of the published X-ray spectrum of XRT 080109 as a purely thermal X-ray breakout spectrum.

In addition to the literal application of both models, it is important to keep in mind the caveats and simplifications that enter them, as both models are consistent with the basic idea of emission from a post-breakout cooling stellar envelope. Any simplifications that lead to a slight misestimation of $T_{\rm BB,ev}$ will lead to a large effect onto $R_\star$ due to its large temperature sensitivity. Caveats here include equating effective temperature (as given by the models) with observed color temperature, and the fact that for temperatures during the time of observations (10^4 K), the opacity is probably not set by simple Thomson scattering as assumed in the models, but is composition dependent (E. Waxman, 2009, private communication). These aspects mark areas of improvement that need to be addressed if measurements like the ones for SN 2008D are to be used to routinely and precisely measure SN progenitor sizes in the future.

For illustration, we overplot in Figure 8 the predicted values for the Waxman model using the parameters put forth by Soderberg et al. (2008b) for SN 2008D, namely $R_\star = 10^{11}$ cm, $M_{\rm ej} = 5\ M_\odot$, and $E_{\rm K} = 2 \times 10^{51}$ erg (see their caption to Figure 3). Our values are consistent with their fits, within the uncertainties. For comparison, we also plot the predicted values for the model of Chevalier & Fransson (2008) with $R_\star = 9\ R_\odot$.

We can now directly compare our estimated $R_\star$ of XRT 080109/SN 2008D with stellar radii of Wolf-Rayet (WR) stars, which possess dense winds (see Abbott & Conti 1987; Crowther 2007 for reviews), and are the most likely progenitors of stripped-envelope SNe (e.g., Filippenko 1991), including that of XRT 080109/SN 2008D (Soderberg et al. 2008b). Specifically, bona fide WN stars—the nitrogen-sequence spectral subtype of WR stars with their helium layer intact but without H (see Smith & Conti 2008 for the distinction between WN and WNH, i.e., H-rich WN stars)—are the likely progenitors of some SNe Ib. Their radii are in the range 1–20 $R_\odot$ with typical sizes between 5 and 10 $R_\odot$ (Herald et al. 2001; Hamann et al. 2006; Crowther 2007). Provided that those models and their data are accurate, $R_\star^{\rm W07} \approx 0.5-1.9\ R_\odot$ as suggested by W07 is smaller by a factor of 5–10 than typical values for such WN radii, while the size of $R_\star^{\rm CF08} = 5$–$20\ R_\odot$ as suggested by CF08 is more in line with data of typical WN stars.

Independent of the considerations above, Soderberg et al. (2008b) infer from their extensive radio observations that the progenitor had a steady wind with a mass-loss rate consistent with those of WR stars.

7. COMPARISON WITH OTHER SUPERNOVAE

The optical signature of postshock breakout, namely a cooling stellar envelope (extremely blue color and dip in the first few days after explosion), has been observed in two stripped-envelope normal SNe: SN IIb 1993J (Schmidt et al. 1993; Richmond et al. 1994) and SN Ib 1999ex (Stritzinger et al. 2002). Other SNe with early-time observations (at $\Delta t \approx 1$ day or earlier) include the broad-lined SN Ic 2006aj connected with low-luminosity GRB/XRF 060218 (Campana et al. 2006, but see Section 9), GRB 980425/SN 1998bw (for the V and R filters, Galama et al. 1998), the famous SN II 1987A (Hamuy et al. 1988), and most recently, two SN II found by the Supernova Legacy Survey and detected with the UV satellite *GALEX* (Schawinski et al. 2008; Gezari et al. 2008).

7.1. Photometry: Cooling Stellar Envelope and Radioactive Decay as Power Sources

Figure 10 compares the optical light curves of SN 2008D with those of other SNe with either observed shock breakout or subsequent phase of cooling stellar envelope emission, where the SNe are offset to match the peak magnitude of SN 2008D in the respective bands. Careful comparison with other stripped-envelope SNe caught shortly (∼1 day) after shock breakout (SN 1993J, SN 1999ex) reveals that while the light curves (and spectra) of SN 2008D and SN 1999ex are similar during the ^{56}Ni-decay phase, the light curves related to the cooling stellar envelope are different among these three SNe. Furthermore, we note that the $B-V$ color evolution of SN 2008D is very similar to that of SN 1999ex during the time of ^{56}Ni decay, but very different during the shock-breakout phase (Figure 11). The color curve of SN 1999ex has a steep rise to and decline from the red during 1 day$< \Delta t < 10$ days, peaking at $B - V = 1$ mag, while that of SN 2008D evolves gradually during this time and reaches $B - V = 0.5$ mag at most.

We leave it as a future topic to model the diversity of the very early-time light curves of SNe 1993J, 1999ex, 2006aj, and 2008D in terms of progenitor radius, $E_{\rm K}$, and $M_{\rm ej}$, and to compare these values with those derived from other methods (e.g., light curve and nebular models). We note, however, that the temporal evolution of the inferred BB temperature and radius of SN 2008D are quite different from those derived for SN 1999ex (Figure 8, the left panel; Stritzinger et al. 2002).

Comparing the light-curve shapes of the different SNe with respect to date of V-band maximum, we find that SN 2008D declines more slowly than any of the other SNe and has a wider peak. One route of parameterizing the SN light-curve shape is

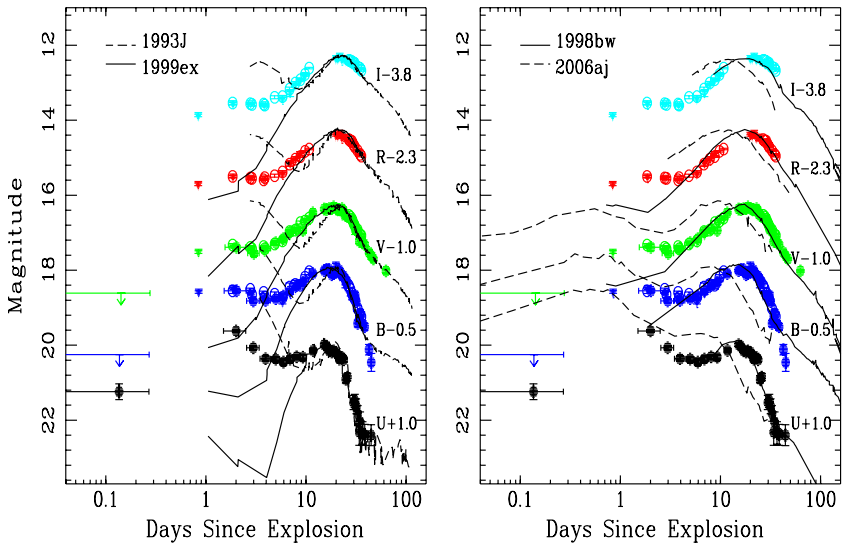

Figure 10. Comparison of the optical *Swift*/UVOT (filled circles) and ground-based (empty circles and triangles) light curves of SN 2008D with those of other normal SNe (*left*) and SNe associated with low-luminosity GRBs (*right*, but see Section 9), for which shock breakout was observed or the time of explosion is well known. Data are from Richmond et al. (1994) for SN1993J, Stritzinger et al. (2002) for SN 1999ex, Galama et al. (1998) for SN 1998bw, and Campana et al. (2006; *UBV*) and Modjaz et al. (2006; $r'i'$) for SN 2006aj. The offsets refer to the *UBVRI* light curves of SN 2008D, while its $r'i'$ light curves are offset by $r' - 2.6$ and $i' - 4.3$ to match *RI*. The rest of the SNe are offset to match the peak magnitude of SN 2008D in the respective bands. For SN 1998bw and SN 2006aj, the SN explosion date was taken to be coincident with the onset of GRB 980425 and XRF 060218, respectively (Galama et al. 1998; Campana et al. 2006). For SN 1993J and SN 1999ex, the explosion dates were estimated from optical nondetections on the night before (for SN 1999ex, JD 2,451,480.5; Stritzinger et al. 2002), and on the night during discovery (for SN 1993J, JD 2,449,074.5 ± 0.05; Wheeler et al. 1993).

(A color version of this figure is available in the online journal.)

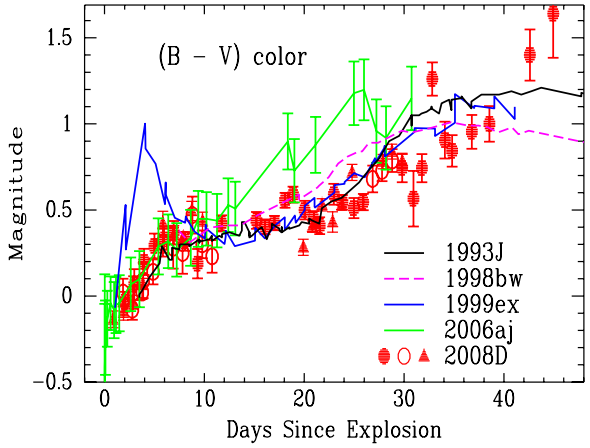

Figure 11. Comparison of the $B - V$ color curve of SN 2008D dereddened by $E(B - V) = 0.6$ mag, with those of other SNe. The $B-V$ color of SN IIb 1993J (Richmond et al. 1994) is dereddened by $E(B - V) = 0.08$ mag (we adopted the lower value derived by Richmond et al. and not their higher alternative of $E(B - V) = 0.28$ mag) and that of SN Ib 1999ex by $E(B - V) = 0.3$ mag (Stritzinger et al. 2002).

(A color version of this figure is available in the online journal.)

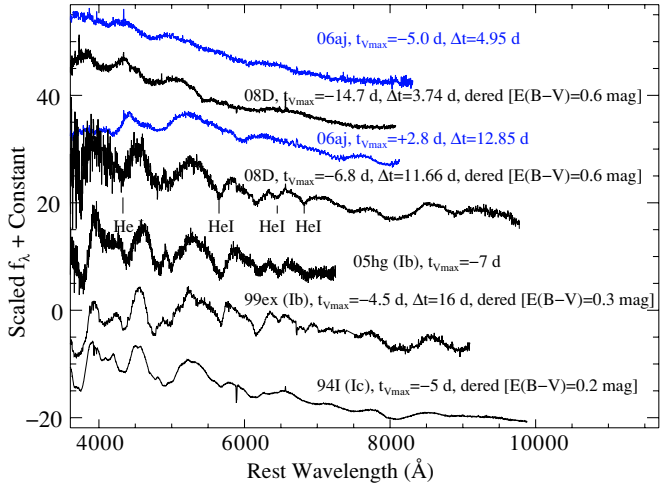

Figure 12. Comparison of the MMT and APO spectra of SN 2008D taken at $\Delta t = 3.74$ days and 11.66 days, respectively, with those of SN 2006aj at similar ages ($\Delta t = 4.95$ and 12.85 days, respectively), and with those of other SN Ib and SN Ic. SN 2006aj was the SN associated with XRF 060218 (Modjaz et al. 2006). The early-time spectra of other SNe Ib and Ic include, dereddened by the indicated amounts: SN 1999ex (Stritzinger et al. 2002; Hamuy et al. 2002), SN 2005hg (Modjaz 2007), and SN Ic 1994I (Filippenko et al. 1995). The optical series of He I lines, defining SN 2008D as an SN Ib, are indicated (namely, He I λλ4471, 5876, 6678, 7061). We note the similarity between SN 2008D and SNe 1999ex and 2005hg.

(A color version of this figure is available in the online journal.)

using the $\Delta m_{15}(X)$ parameter, a formalism initially developed for SNe Ia (Phillips 1993), which is defined as the decline (in magnitudes) during the first 15 days after maximum brightness in the passband X. For SN 2008D, we measure $\Delta m_{15}(U) = 1.2$ mag, $\Delta m_{15}(B) = 0.8$ mag, and $\Delta m_{15}(V) = 0.6$ mag.

7.2. Optical Spectroscopy: Emergence of He I Lines

The very early spectra ($\Delta t \approx 3$–5 days) actually resemble those of SN 2006aj (see the top two spectra in Figure 12; see also Mazzali et al. 2008; Malesani et al. 2009), the SN connected with GRB/XRF 060218, which initially led to the identification of this SN as a broad-lined SN (Blondin et al. 2008b; Kong et al. 2008a, but see Malesani et al. 2008). This spectral resemblance suggests that in both systems, the material constituting the photosphere at early times is at high velocity (Mazzali et al. 2008), as expected from homologous expansion. Indeed, the velocity we determined via SYNOW, $v_{\rm phot} \approx 30{,}000$ km s^{-1} at $\Delta t = 1.8$ days in the spectrum with the double-absorption feature (see Section 5.3), is similar to those of broad-lined SNe Ic at the same epoch measured in a slightly different manner (Mazzali et al. 2008).

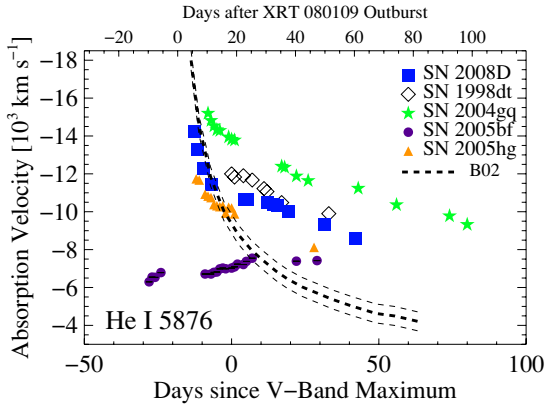

Figure 13. Temporal velocity evolution of He I λ5876 in SNe Ib: SN 1998dt (Matheson et al. 2001), SN 2005bf (Tominaga et al. 2005; Modjaz 2007), SN 2004gq and SN 2005hg (Modjaz 2007), and SN 2008D (this work). He I λ 5876 is usually the strongest He I line. The absorption velocities decrease over time, except for the maverick SN Ib 2005bf (see text). The velocities for SN 2008D lie within the range of observed values, with the earliest measurements before maximum for a normal SN Ib. The thick dashed line is the functional form for the photospheric velocity as fit by Branch et al. (2002; B02) to SN Ib data. The thin dashed lines demarcate the extent in their uncertainty. See text for details.

(A color version of this figure is available in the online journal.)

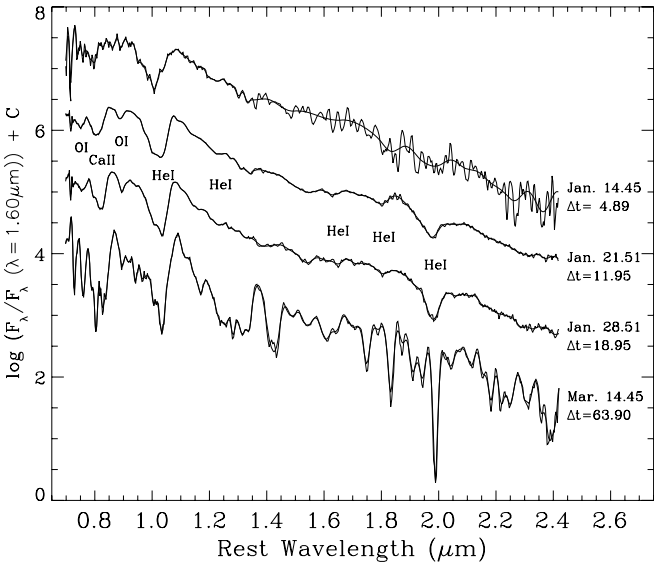

Figure 14. Three NIR spectra of SN 2008D taken with the IRTF. The dates of observation are indicated, along with SN ages (Δt) with respect to time of shock breakout (in days). The five detected He I lines are indicated by their rest wavelengths. The spectra are shown as both raw and Fourier smoothed, and are normalized and offset by arbitrary amounts for clarity. Note the strong presence of blueshifted He I 1.0830 at ∼1.02–1.05 μm and blueshifted He I 2.0581 μm at ∼1.97–1.98 μm. The broad absorption at 1.05 μm probably includes an additional blend of other lines (mostly Fe II, but also Mg II, C I, and Si I).

However, while SN 2006aj and other broad-lined SNe Ic continue to have a significant amount of mass at high velocity (at least 0.1 $M_\odot$ at 20,000–30,000 km s^{-1} of the total of 2 $M_\odot$ ejected mass as derived from models in Mazzali et al. 2006), at $\Delta t \approx 12$ days, the receding photosphere in SN 2008D reveals the lower-velocity layers and the development of He I lines which SN 2006aj and other broad-lined SNe Ic do not show (Figure 12). Spectral synthesis modeling yields an estimate of ∼0.03 $M_\odot$ at $v > 0.1c$ for SN 2008D (Mazzali et al. 2008; Tanaka et al. 2009), a factor of 10–50 less than for GRB-SNe.

As Figure 12 shows, the later spectral evolution of SN 2008D resembles that of a normal SN Ib, where the He I lines are as pronounced as in SN 2005hg and more so than in SN 1999ex.

We now investigate the temporal behavior of the He I lines, which are the spectral hallmarks of SNe Ib. In SN 2008D and in a larger sample of SNe Ib, we determine the blueshifts in the maximum absorption in the He I lines via the robust technique of measuring SN line profiles as presented by Blondin et al. (2006).

We refer to our velocity measurements as "He I absorption-line velocities" in the rest of this work. In Figure 13 (see also Table 9), we present the measured values for He I λ 5876, the strongest optical He I line in SN 2008D, along with absorption-line velocities of a sample of other SNe Ib (see Modjaz 2007), measured in the same fashion.

In SN 2008D, the He I lines become apparent as early as $\Delta t \approx 6$ days (i.e., $t_{V\max} \approx -13$ days) and are fully identified at $\Delta t \approx 11.7$ days ($t_{V\max} \approx -6.9$ days). Figure 13 reveals that the velocities span a large range for normal SNe Ib; e.g., at maximum light, they range from −14,000 km s^{-1} (for SN 2004gq) to ∼−10,000 km s^{-1} (for SN 2005hg), and seem to follow a power-law decline. For comparison, Branch et al. (2002) showed that the He I velocities in the SNe Ib of their limited sample followed a standard pattern and traced fairly closely (within 2000 km s^{-1} for the same epoch) the photospheric velocities derived from synthetic fits to Fe II lines, which we overplot in Figure 13 (dashed line, using their power-law fit $v_{\rm phot} \propto t^{-2/(n-1)}$ with $n = 3.6$). However, the SNe Ib in our sample show a larger departure (up to 6000 km s^{-1}) from the corresponding standard photospheric velocity, larger than those of SN 1998dt, which Branch et al. (2002) had declared as the exception in their sample. In addition, both SNe 2008D and 2005hg show He I line velocities that are *lower* than the corresponding photospheric velocity for dates before maximum light. This might mean that the line-emitting material is located at radii smaller than the bulk of the material that makes up the photosphere, or that there are optical-depth effects at play.

It has been long suggested that the He I lines are due to nonthermal excitation and ionization of gamma-ray photons produced during the radioactive decay of ^{56}Ni and ^{56}Co (Harkness et al. 1987; Lucy 1991; Mazzali & Lucy 1998). The fact that the gamma-ray photons need time to diffuse through the ejecta to reach the He layer has been invoked to explain the late emergence (after maximum light) of He I in some SNe Ib (e.g., Filippenko 1997, and references therein). A challenge for those who study the complicated nonthermal excitation effects in SN line formation (Baron et al. 1999; Kasen et al. 2006; Dessart & Hillier 2008) would be to self-consistently explain for SN 2008D its early emergence of He I lines (∼5–6 days after explosion, and ∼12–13 days before maximum light) by excitation of the relatively small amount of synthesized ^{56}Ni (0.05–0.1 $M_\odot$, Soderberg et al. 2008b; Mazzali et al. 2008; Tanaka et al. 2009).

7.3. NIR Spectroscopy as a Possible Discriminant

Figure 14 shows the four NIR spectra of SN 2008D (taken with the IRTF) in which we detect five prominent blueshifted He I lines. We tabulate their velocities as inferred from maximum absorption in Table 9.

Comparison of the NIR spectra of proper SNe Ib 1999ex, 2001B, and 2008D with those of SNe Ic (see Taubenberger et al. 2006 and references therein) shows that all SNe display a strong feature at ∼1.04 μm but *only* SNe Ib show additional absorption at 1.95–2.0 μm due to blueshifted He I 2.058 μm, while none of the SNe Ic do. For the few SNe Ib in general (Gerardy et al. 2004) and for SN 2008D in particular, the absorption velocity of

Table 9
Optical and Near-Infrared He I Absorption-line Velocities of SN 2008D

JD−2,400,000 (day)	Δt (day)	$t_{V\max}$ (day)	He I λ5876 (km s^{-1})	He I λ6678 (km s^{-1})	He I λ7065 (km s^{-1})	He I 1.0830 μm (km s^{-1})	He I 2.0581 μm (km s^{-1})
54479.96	4.89	−13.6	...	...	...	−21,700[a]	−14,200
54480.82	5.75	−12.7	−14,200	−11,800	−10,500	...	...
54481.84	6.77	−11.7	−13,300	−12,700	−13,000	...	...
54484.07	9.00	−9.4	−12,300	−12,400	−10,900	...	...
54486.72	11.66	−6.8	−11,500	−11,100	−10,500	...	...
54487.01	11.95	−6.5	...	...	...	−14,900	−12,200
54494.01	18.95	0.5	...	...	...	−13,900	−11,700
54497.85	22.78	4.3	−10,600	−10,400	−10,100	...	...
54498.94	23.88	5.4	−10,600	−10,200	−10,200	...	...
54505.62	30.56	12.1	−10,500	−10,200	−9900	...	...
54507.68	32.61	14.2	−10,400	−10,000	−9900	...	...
54508.93	33.87	15.4	−10,300	−9900	−9700	...	...
54512.86	37.79	19.4	−10,000	−9600	−9500	...	...
54524.87	49.81	31.4	−9300	−8600	−8700	...	...
54535.73	60.67	42.2	−8600	−7900	−8100	...	...
54539.0	63.92	45.5	...	...	...	−13,900	−10,200

Note. [a] Likely due to a blend and not traced by He I.

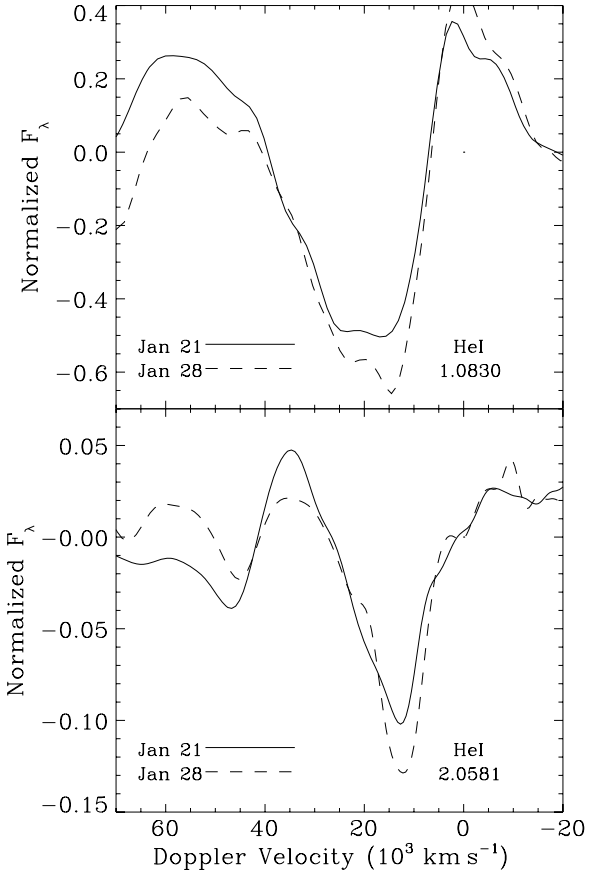

Figure 15. Two main helium lines detected in NIR spectra of SN 2008D in velocity space for two epochs: 2008 January 21.51 (Δt = 11.95 days; solid lines) and January 28.51 (Δt = 18.95 days; dashed lines). The top plot shows the NIR spectra with respect to He I 1.083 μm as zero velocity, and the bottom one with respect to He I 2.058 μm. The largest difference between the two lines is the effect of blending of other elements with the He I 1.083 μm line. The blueshifted He I 2.058 μm line is narrower and more well defined than the blend around 1 μm, of which we take the red absorption trough to be due to He I 1.083 μm. Both He I lines have similar velocities based on the blueshifted maximum absorption (see Table 9). The spectra are normalized to the local continuum.

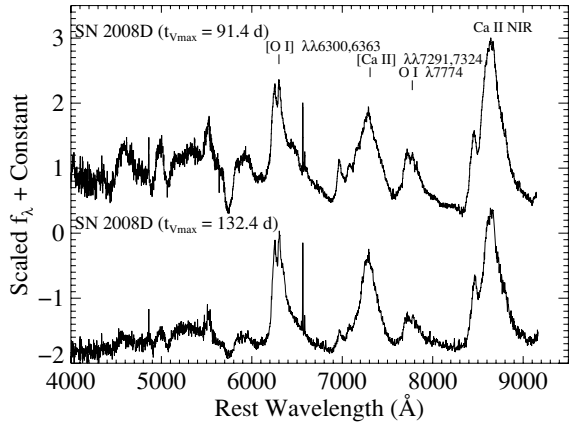

Figure 16. Spectra of SN 2008D at three and four months after maximum light (2008 April 28, and June 7). The main emission lines in the spectrum are marked, and their rest wavelengths are indicated. We caution that the line at 7300 Å could be a blend of [O II] λλ7319, 7330 and some Fe lines, in addition to [Ca II] λλ7291, 7324, as marked.

the strong blueshifted He I 2.058 μm is very similar to the strong blueshifted He I 1.083 μm if we identify the redder absorption trough of the multicomponent feature at 1 μm as He I 1.083 μm. As Figure 15 shows, the blueshifted He I 2.058 μm line is narrower and more well defined than the broad blend at 1 μm.

In conclusion, SN 2008D gives supporting evidence to the argument that the broad absorption at ∼1.04 μm is a poor diagnostic for helium, since it is most likely a blend of Fe II, C I, Ca II, and S I at the same wavelengths (Millard et al. 1999; Gerardy et al. 2004; Sauer et al. 2006) and He I in SNe Ib. However, claims of significant He in optically classified SN Ic rely on identifying the same strong absorption feature at ∼1.04 μm exclusively with He I 1.083 μm (Filippenko et al. 1995; Clocchiatti et al. 1996; Patat et al. 2001). Our study of SN 2008D implies that determining unambiguously if indeed helium is present in SNe normally classified as Type Ic requires a *K*-band spectrum to test for the presence of the clean and unblended He I 2.058 μm feature.

8. DOUBLE-PEAKED OXYGEN LINES AND ASPHERICAL EXPLOSION GEOMETRY

In Figure 16, we present the Keck spectra of SN 2008D taken at $t_{V\max}$ = 91.4 days (i.e., Δt = 109 days) on 2008 April 28,

and $t_{V\max} = 132.4$ days, on 2008 June 7. They show nebular emission lines on top of some residual, underlying photospheric spectrum, which is more pronounced in the earlier spectrum. This is expected, as SNe appear to turn fully transparent ~200 days after maximum light, and some SNe take up to one year to complete the transition (Mazzali et al. 2004). Here, we are witnessing this transition period for SN 2008D. Below, we analyze the nebular emission lines of SN 2008D.

At sufficiently late times, the SN ejecta become fully optically thin in the continuum; hence, spectra obtained during this time period afford a deeper view into the core of the explosion than spectra taken during the early photospheric phase. In the absence of hydrogen, oxygen is the primary coolant in the ejecta of stripped-envelope SNe at late epochs when the gas is neutral or at most singly ionized (Uomoto & Kirshner 1986; Fransson & Chevalier 1987), and when densities are sufficiently low for forbidden lines to be the strongest ones in the spectrum. In SN 2008D, we detect [O I] λλ6300, 6363 and O I λ7774 along with [Ca II] λλ7291, 7324 and the strong Ca II NIR triplet.

To study the line profiles of SN 2008D more closely, we plot the main relatively unblended emission lines ([O I] λλ6300, 6363, O I λ7774, and [Ca II] λλ7291, 7324) in velocity space in Figure 17. The two oxygen lines show the same unusual double-peaked profile, while [Ca II] λλ7291, 7324 does not exhibit it. For both oxygen lines, the redder peak is at zero velocity, and the trough between the two peaks is shifted by ~ -800 km s^{-1} from zero velocity. The total separation between the two peaks is ~2000 km s^{-1} for both the forbidden and the permitted oxygen lines. With the chosen zero point for [Ca II] λλ7291, 7324 (namely 7307.5 Å, the straight mean of the two calcium lines), its peak is also blueshifted by ~800 km s^{-1}, but blending with other lines ([O II] λλ7319, 7330, Fe) could be affecting the line shape and the exact determination of zero velocity.

While optical-depth effects sometimes generate double-peaked [O I] λλ6300, 6363 because of its doublet nature (most notably in SN 1987A; Spyromilio 1991; Leibundgut et al. 1991; Li & McCray 1992), it is not the culprit in SN 2008D, since (a) the separation of the doublet (3000 km s^{-1}) is larger than the observed separation between the double peaks (2000 km s^{-1}), and (b) O I λ7774, a multiplet with very small separations (at most 3 Å, i.e., 130 km s^{-1}, smaller than our spectral resolution), shows the same double-peaked profile as [O I] λλ6300, 6363 in SN 2008D. The [Ca II] λλ7291, 7324 line does not show the same double-peaked profile, but this may well be because the emission comes from smoothly distributed, preexisting (natal) calcium similar to what was seen in SN IIb 1993J (Matheson et al. 2000a).

Such double-peaked oxygen emission lines have recently been observed in a number of stripped-envelope SNe (Mazzali et al. 2005; Maeda et al. 2007; Modjaz et al. 2008c; Maeda et al. 2008; Taubenberger et al. 2009), and have been interpreted in the framework of global asphericities, where the emitting oxygen-rich ejecta are situated in a ring- or torus-like structure viewed along the equatorial plane. Both Modjaz et al. (2008c) and Maeda et al. (2008) suggest that such global asphericities are common during core collapse. Maeda et al. (2008) specifically suggest that their observed fraction of double-peaked profiles (40% ± 10%) is consistent with the hypothesis that all stripped core-collapse events are mildly aspherical, given their models in Maeda et al. (2006), whereas Taubenberger et al. (2009) find a lower observed fraction (5%–18%). Recently, Milisavljevic et al. (2009) have argued that it is difficult to explain all line profiles observed in their recent SN sample via purely geometric

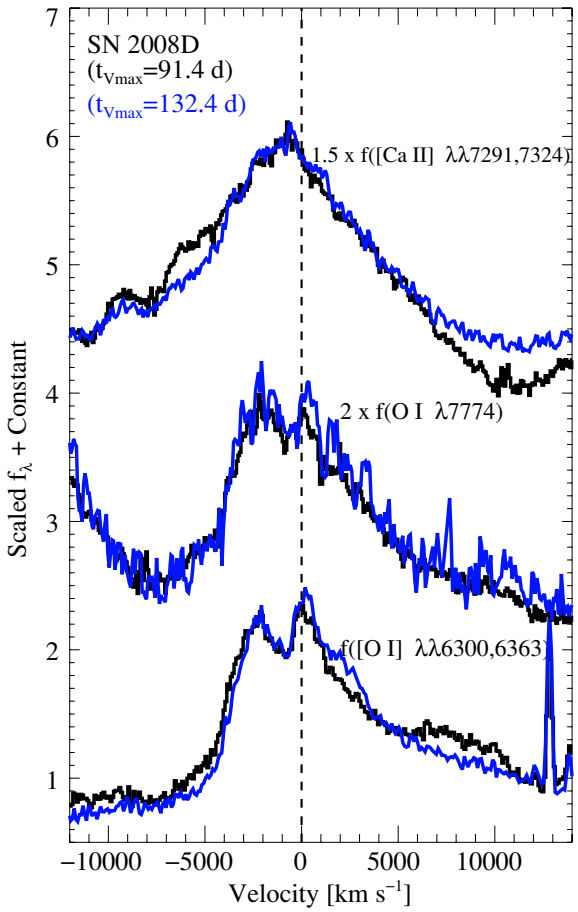

Figure 17. Main late-time emission lines of SN 2008D in velocity space in the rest frame of NGC 2770. The zero point for [O I] λλ6300, 6363 here is 6300 Å, while that of [Ca II] λλ7291, 7324 is taken at 7307.5 Å (straight mean of the two calcium lines). We caution that [Ca II] might be a blend with [O II] and Fe. Zero velocity is indicated by the dashed line. The two oxygen lines show the same conspicuous double-peaked profile, indicating that the two horns cannot be due to the doublet nature of [O I] λλ6300, 6363. In both cases, the redder peak is at zero velocity, and the trough between the two peaks is shifted by ~ -800 km s^{-1} from zero velocity for both spectra. With the chosen zero point for [Ca II] λλ7291, 7324, its peak is also blueshifted by ~800 km s^{-1}, though blending could be affecting the line shape and the exact location of zero velocity. See text for more details.

(A color version of this figure is available in the online journal.)

effects. However, their conclusions only concern SNe whose double-peaked profile has a velocity separation close to that of the doublet [O I] λλ6300, 6363 and does not show it in lines other than the doublet; those features are not observed in SN 2008D (see Figure 16 and above).

While other SNe IIb and Ib have been shown to exhibit some small-scale structure in oxygen, indicating some clumping in the density distribution of oxygen probably due to instabilities (Filippenko & Sargent 1986; Spyromilio 1994; Sollerman et al. 1998; Matheson et al. 2000a; Elmhamdi et al. 2004), the clear symmetric double peaks in SN 2008D are different and may rather indicate a global scale for the anisotropy. The mechanism giving rise to such a global anisotropy could lie in the intrinsic explosion physics of core collapse, since each of the various theoretical core-collapse models, be it neutrino driven (Scheck et al. 2006), acoustic (Burrows et al. 2006), or magneto driven (Burrows et al. 2007; Dessart et al. 2008), finds that symmetry breaking is essential for a successful explosion.

Alternatively, in case the progenitor of SN 2008D is part of a binary, binary interaction or a merger might be modulating

the geometry of the explosion, though this speculation will be very hard to verify. Nevertheless, other lines of evidence such as polarization studies of SNe II, Ib, and Ic (e.g., Leonard & Filippenko 2005), neutron-star kick velocities (Wang et al. 2006), and young SN remnant morphologies (e.g., Cas A; Fesen et al. 2006) suggest that asphericities are generic to the core-collapse process.

We note the blueshift from zero velocity (of the order ∼800 km s^{-1}, Figure 17) in the oxygen trough, if the trough between the two peaks is regarded as the symmetry center. The same blueshift might also be present in the calcium peak, depending on the choice of zero velocity, which is more uncertain than for the oxygen lines due to possible blending with other lines. This blueshift, if real, could be caused by residual opacity before reaching the full nebular phase (Taubenberger et al. 2009), peculiar distribution of ^{56}Co which is powering the emission at such later epochs, large-scale asymmetry, or offset of the SN rest-frame velocity from that of NGC 2770 by 800 km s^{-1}. However, given that the rotation curve of the host galaxy, NGC 2770, extends to only ∼400 km s^{-1} (Haynes et al. 1997), the last option is least likely.

Future multi-epoch late-time spectra (especially those taken at $t_{V\max} \gtrsim 200$ days) are needed to differentiate between the various scenarios as each one predicts a different behavior of the blueshift over time. If it is due to residual opacity, the most probable case, we predict that the blueshift will go to zero for spectra at $t_{V\max} \gtrsim 200$ days. We can exclude dust formation as the culprit, since the apparent blueshift does *not* increase over time, contrary to the behavior of blueshifted lines in SN where dust had been formed (e.g., Smith et al. 2008). If the blueshift continues to remain constant over time (as seen in SN 1996N; Sollerman et al. 1998), then bulk blueshifts or unipolar blob ejections might need to be invoked as suggested for SN 2005bf (Maeda et al. 2007).

In summary, we infer from the presence of double peaks in the two different oxygen lines in SN 2008D that global asphericities were probably involved during the explosive event of SN 2008D, regardless of the specific mechanism that actually leads to a successful explosion.

9. X-RAY INTERPRETATION

The origin of the X-ray emission of XRT 080109 is highly debated. Soderberg et al. (2008b) and Chevalier & Fransson (2008) attribute it fully to the processes related to core-collapse shock-breakout emission, while others (Xu et al. 2008; Li 2008; Mazzali et al. 2008) claim it as emission caused by a stifled or weak GRB jet. Soderberg et al. (2008b) adopt the pure power-law X-ray spectrum fit and use the calculations of Wang et al. (2007) to explain the power-law shape in terms of upscattering (i.e., Comptonization) of thermal shock breakout photons with energies < 0.1 keV by the circumstellar wind medium. On the other hand, Chevalier & Fransson (2008) favor the pure blackbody fit and explain the artificially small BB radius as the product of a scattering atmosphere, where the emission is generated in a relatively deep layer but effectively emitted at a larger radius. Even for XRF 060218/SN 2006aj, which had a much higher S/N spectrum, the exact origin of the X-ray emission is still debated (Campana et al. 2006; Ghisellini et al. 2007; Soderberg et al. 2006; Waxman et al. 2007).

While the above authors attempt to test the system of XRT 080109 for emission from relativistic ejecta, their conclusions differ and are heavily model dependent. In the next section, we explore a phenomenological approach where we compare the observed properties of XRT 080109 with those of so-called X-ray flashes (Heise et al. 2001), high-energy transient that are likely softer analogs of cosmological GRBs (Sakamoto et al. 2008). We note that, recently, Bietenholz et al. (2009) find no evidence for a relativistic, off-axis jet in SN 2008D based on their VLBI observations of SN 2008D. Very recently, Katz et al. (2009) have argued that nonthermal X-ray spectra may be common during the breakout of radiation-mediated nonrelativistic shocks, as suggested to be the case for XRT 080109.

9.1. Comparison with X-ray Flashes

Here we compare three properties of XRT 080109 with those observed in a sample of classical XRFs: duration (as parameterized by T_{90}), the shape of the X-ray spectrum, and X-ray-to-optical flux ratio. In addition, we discuss its energy output.

While in each case XRT 080109 is not necessarily an obvious outlier in the observed distribution, together all three considerations paint a strong picture that XRT 080109, along with XRF 060218/SN 2006aj, might be different phenomenologically from the rest of classical XRFs. However, future studies trying to uncover the inherent distribution will need to carefully consider detector effects and rest-frame properties.

1. *Duration*: XRFs observed by HETE-2 and *Swift* are seen to have similar temporal profiles and durations compared to long-duration GRBs, exhibiting a FRED (i.e., fast rise exponential decline) profile. XRT 080109 can be adequately fit by such a FRED profile (Section 9.1), but the transient's duration is an order of magnitude longer than the median T_{90} for other XRFs and X-ray-rich GRBs (XRRs), which is roughly 30 s (Sakamoto et al. 2005, 2008). Both XRT 080109 and XRF 060218/SN 2006aj have the longest durations ($T_{90} = 470 \pm 30$ s and 2100 ± 100 s, respectively). We note the caveat that satellites are typically inhibited from triggering on long timescales due to background modulations, and XRT 080109 could not have been detected with any other survey X-ray telescope before *Swift*.
2. *X-ray spectrum*: XRF 060218/SN 2006aj has a significant X-ray component that (a) is thermal and (b) appears to soften over time, with very high S/N (Campana et al. 2006; Butler 2007a). The X-ray spectrum of XRT 080109 is of much lower S/N, and is well fit by a combined PL+BB (Section 2). While the X-ray emission of XRF 060218 fades at a rate comparable to that often observed for GRB X-ray afterglows, its spectrum is markedly softer (e.g., Soderberg et al. 2006) and also softens strongly in time (Butler 2007a). This is in contrast to GRB X-ray afterglows, which exhibit little spectral evolution at the same epoch: GRB and XRF X-ray afterglows have photon indices of $\Gamma \approx 2$, while that of XRF 060218/SN 2006aj was $\Gamma = 3.41 \pm 0.13$ (Butler & Kocevski 2007b). There is evidence that the XRT 080109 late-time X-ray spectrum (from the *Chandra* data) was also softer with $\Gamma = 3.6^{+1.7}_{-1.4}$ (Pooley & Soderberg 2008; Soderberg et al. 2008b) than the early-time spectrum.
3. We also compare the radiation output in XRT 080109 for different wavelengths with that of XRFs and their afterglows.

At the dates of our optical and NIR photometry (at $t - t_o = \Delta t = 0.84$ and 0.71 day, i.e., ∼70 and 60 ks), the X-ray luminosity is in the range $\sim 2 \times 10^{38-39}$ erg s^{-1}. Thus, the X-ray luminosity (for 0.3–10.0 keV) is 3–4 orders of magnitude

lower than the luminosity inferred from the optical observations (see Section 6.1); thus, $L_X/L_{opt} \approx 10^{-3}$to 10^{-4} at 70 ks for XRT 080109/SN 2008D. This corresponds to a ratio of fluxes $f_{O/X} = 4 \times (10^2$–$10^3)$, while the observed ratio is $f_{O/X} < 70$ for classical XRF afterglows (D'Alessio et al. 2006) and GRB afterglows (De Pasquale et al. 2003) at comparable times (using the same definition and units of $f_{O/X}$ as in D'Alessio et al. 2006). In other words, the optical to X-ray ratio for XRT 080109/SN 2008D is a factor of $\sim 10^3$ larger than for XRF afterglows. For XRF 060218/SN 2006aj, the ratio cannot be precisely determined since it was not observed in the desired bandpass at such early time.

The two main features commonly observed in XRFs are not measured for XRT 080109, namely detection of gamma-ray emission and peak of the energy distribution (E_{peak}).

In summary, XRT 080109, along with XRF 060218/SN 2006aj, appears qualitatively different from the observed distribution of classical XRFs, when considering all three discussed properties together (duration, spectral evolution, and optical to X-ray ratio). Finally, the prompt high-energy emission released in XRT 080109 ($E_{X,iso} \approx 6 \times 10^{45}$ erg) is 3–4 orders of magnitude lower than in XRFs (Soderberg et al. 2008b).

10. CONCLUSIONS

We have presented extensive early-time photometric (*UVW2*, *UVM2*, *UVW1*, *UBVRr′Ii′JHK$_s$*) and spectroscopic (optical and NIR) data on SN 2008D as well as X-ray data analysis on the associated XRT 080109. Our data span a time range of 5 hr before the detection of the X-ray transient to 150 days after the detection and establish that SN 2008D is a spectroscopically normal SN Ib at maximum light, with a relatively long rise time (18 days) and a modest optical peak luminosity of $M_V = -17.0 \pm 0.3$ mag and $M_B = -16.3 \pm 0.4$ mag, after correcting for $E(B-V)_{Host} = 0.6 \pm 0.1$ mag.

We also present the earliest NIR (*JHK$_s$*) detections (at 0.71 day). Our densely time-sampled optical spectral sequence, along with our NIR spectra, uncovers the epoch at which the helium lines emerge. The early-time spectra reveal high expansion velocities (15,0000–30,000 km s^{-1}) up to 6–7 days after outburst, and one specific spectrum (at $\Delta t = 1.84$ days) shows a transient, prominent double-absorption feature at blue wavelengths ($\sim$4000 Å) that is no longer visible in spectra taking 1 day later. In spectra taken three and four months after maximum light, we detect double-peaked profiles in the oxygen lines that we take to indicate global asphericities in the SN core ejecta, and argue that they cannot be due to optical-depth effects. Furthermore, we recommend for future searches for helium in SNe Ic that *J*- and *K*-band spectra are obtained to test for the presence of both He I 1.083 μm and He I 2.058 μm.

The comprehensive data presented here allow us to construct a reliable measurement of the bolometric output for this stripped-envelope SN, including UV and NIR contributions that are usually lacking for other SNe. For data $\Delta t > 3$ days, we find that the bolometric luminosity based on direct *UVW1* $\rightarrow$ K_s integration is very similar to that based on the blackbody fits to the broadband photometry (within $\lesssim$0.04 dex or $\lesssim$ 8%), such that the UV-NIR emission of SN 2008D may well be described by that of a blackbody. We furthermore compare our early-time light curves to fits by Soderberg et al. (2008b), who use the calculations of Waxman et al. (2007) for the cooling stellar envelope blackbody model, and test the predictions of the alternative cooling envelope model of Chevalier & Fransson (2008). Combining our comprehensive data with estimates of E_K and M_{ej} from the literature, we estimate the stellar radius $R_\star$ of its probable Wolf–Rayet progenitor. According to the models of Waxman et al. (2007) and Chevalier & Fransson (2008), we derive $R_\star^{W07} = 1.2 \pm 0.7\ R_\odot$ and $R_\star^{CF08} = 12 \pm 7\ R_\odot$, respectively. The larger size of the progenitor of SN 2008D based on the model of Chevalier & Fransson is somewhat more consistent with typically observed radii of WN stars than the size required by the Waxman model.

Furthermore, we find that the *Swift* X-ray spectrum can be fit equally well by an absorbed power law or a superposition of about equal parts of both power law and blackbody, which has not been suggested before in the literature and has implications for determining the mechanism of the X-ray emission. Specifically, our derived blackbody radius from the PL+BB fit is larger (by a factor of 10) than that of Mazzali et al. (2008), whose jet interpretation of the origin of the X-ray emission is largely based on the small inferred BB area.

XRT 080109 is different from the apparent distribution of classical X-ray flashes as evidenced by its long duration, softening of the X-ray spectrum, and very high optical to X-ray luminosity ratio, though future studies of the inherent distribution will need to fold in detector effects and consider rest-frame properties. Future detections are expected to show unambiguously whether these two events are part of a continuous distribution of XRFs or members of a different physical class of events.

Additional multi-epoch late-time observations (especially for more than 200 days after maximum light) of SN 2008D will be useful to monitor the behavior of the double-peaked oxygen lines and their associated possible blueshift, and, as the SN becomes fully transparent, allow for closely constraining the geometry of the explosion as revealed by the core ejecta. Moreover, such observations are important to monitor for any late-time interactions between SN ejecta and the presumably prior-shed hydrogen envelope to further study the mode of mass loss and search for episodes of sudden mass loss.

M.M. thanks Roger Chevalier, Phil Chang, Chris Matzner, Peter Nugent, Alceste Bonanos, Andrew MacFadyen, and Tsvi Piran for enlightening discussions. R.P.K. thanks Eli Waxman for helpful comments. M.M. is supported by a fellowship from the Miller Institute for Basic Research in Science. We thank S.S. Piatek, T. Pryor, and E. Olszewski for obtaining a few of the spectra presented here. Some of the observations reported here were obtained at the MMT Observatory, a joint facility of the Smithsonian Institution and the University of Arizona, and at the W.M. Keck Observatory, which was made possible by the generous financial support of the W.M. Keck Foundation. We wish to extend special thanks to those of Hawaiian ancestry on whose sacred mountain we were privileged to be guests. The Apache Point Observatory 3.5 m telescope is owned and operated by the Astrophysical Research Consortium. This work is based in part on observations obtained at the Gemini Observatory, which is operated by the Association of Universities for Research in Astronomy, Inc., under a cooperative agreement with the National Science Foundation (NSF) on behalf of the Gemini partnership: the NSF (US), the Particle Physics and Astronomy Research Council (UK), the National Research Council (Canada), CONICYT (Chile), the Australian Research Council (Australia), CNPq (Brazil), and CONICET (Argentina).

PAIRITEL is operated by the Smithsonian Astrophysical Observatory (SAO) and was made possible by a grant from the Harvard University Milton Fund, a camera loan from the University of Virginia, and continued support of the SAO and UC Berkeley. The PAIRITEL project is further supported by NASA/*Swift* Guest Investigator grant NNG06GH50G. KAIT was made possible by generous donations from Sun Microsystems, Inc., the Hewlett Packard Company, AutoScope Corporation, Lick Observatory, the NSF, the University of California, and the Sylvia and Jim Katzman Foundation. We also thank the TABASGO Foundation for continued support. H.M. is a visiting astronomer at the Infrared Telescope Facility, which is operated by the University of Hawaii under Cooperative Agreement no. NCC 5–538 with the National Aeronautics and Space Administration (NASA), Science Mission Directorate, Planetary Astronomy Program. N.R.B. is supported through the GLAST Fellowship Program (NASA Cooperative Agreement: NNG06DO90A).

Supernova research at UC Berkeley is supported in part by the TABASGO Foundation and NSF grant AST-0607485 to A.V.F. Supernova research at Harvard University is supported by NSF grant AST-0606772 to R.P.K. D.P. and N.R.B. were partially supported through the DOE SciDAC grant DE-FC02-06ER41453. J.S.B. was partially supported by the Hellman Faculty Fund. J.X.P. is partially supported by NASA/*Swift* grants NNG06GJ07G and NNX07AE94G and an NSF CAREER grant (AST-0548180). Work by W.H.dV. and S.S.O. was performed under the auspices of the U.S. Department of Energy by Lawrence Livermore National Laboratory under Contract DE-AC52-07NA27344. G.S.S. wishes to thank M. Drosback, B. Keeney, M. Moe, and K. O'Malia for relinquishing some APO time of the University of Colorado, S. Hawley for awarding APO Director's Discretionary Time, R. McMillan for "a little more time" to complete the data acquisition in one night, and the APO Observing Specialists for their assistance. G.S.S. is partially supported by NASA grants NNX06AG43G and NNX06AG44G, and B.P.H. and G.D.I. are partially supported by NASA grant NAG5-7697. C.H.B. acknowledges support from the Harvard Origins of Life Initiative. H.M. and P.G. thank Alan Tokunaga for arranging the IRTF observations on short notice.

This research has made use of NASA's Astrophysics Data System Bibliographic Services (ADS) and the NASA/IPAC Extragalactic Database (NED), which is operated by the Jet Propulsion Laboratory, California Institute of Technology, under contract with NASA. We thank the *Swift* team and the observers who provided their data and analysis through the GCN. We collectively thank the staffs of the MMT, APO, Keck, Lick, and Gemini Observatories for their assistance. We thank the http://arXiv.org server that made it possible to communicate our results to the interested reader in a timely fashion.

Facilities: Swift, KAIT, FLWO: 1.2 m, Nickel, PAIRITEL, Keck: I (LRIS), Keck: I (HIRES), Keck: II (DEIMOS), Gemini: South (GMOS-S), Magellan: Clay (LDSS-3), MMT (Blue Channel spectrograph), Shane (KAST), ARC: APO (DIS), FLWO: 1.5 m (FAST), IRTF (SpeX)

REFERENCES

Abbott, D. C., & Conti, P. S. 1987, ARA&A, 25, 113
Alard, C. 2000, A&AS, 144, 363
Alard, C., & Lupton, R. H. 1998, ApJ, 503, 325
Baron, E., Branch, D., Hauschildt, P. H., Filippenko, A. V., & Kirshner, R. P. 1999, ApJ, 527, 739
Berger, E., & Soderberg, A. 2008, GCN Circ. 7159
Bietenholz, M. F., Soderberg, A. M., & Bartel, N. 2009, ApJ, 694, L6
Blinnikov, S., Lundqvist, P., Bartunov, O., Nomoto, K., & Iwamoto, K. 2000, ApJ, 532, 1132
Blinnikov, S. I., Eastman, R., Bartunov, O. S., Popolitov, V. A., & Woosley, S. E. 1998, ApJ, 496, 454
Blondin, S., Matheson, T., Modjaz, M., & Berlind, P. 2008a, Central Bureau Electronic Telegrams, 1205, 1
Blondin, S., Matheson, T., Modjaz, M., & Berlind, P. 2008b, Central Bureau Electronic Telegrams, 1205, 1
Blondin, S., et al. 2006, AJ, 131, 1648
Blondin, S., et al. 2008c, IAU Circ., 8908, 2
Bloom, J. S., et al. 2006, in ASP Conf. Ser. 351, Astronomical Data Analysis Software and Systems XV, ed. C. Gabriel et al. (San Francisco, CA: ASP), 751
Branch, D., et al. 2002, ApJ, 566, 1005
Branch, D., Jeffery, D. J., Young, T. R., & Baron, E. 2006, PASP, 118, 791
Burrows, A., Dessart, L., Livne, E., Ott, C. D., & Murphy, J. 2007, ApJ, 664, 416
Burrows, A., Livne, E., Dessart, L., Ott, C. D., & Murphy, J. 2006, ApJ, 640, 878
Burrows, D. N., et al. 2005, Space Sci. Rev., 120, 165
Butler, N. R. 2007a, ApJ, 656, 1001
Butler, N. R. 2007b, AJ, 133, 1027
Butler, N. R., & Kocevski, D. 2007a, ApJ, 663, 407
Butler, N. R., & Kocevski, D. 2007b, ApJ, 668, 400
Butler, N. R., et al. 2006, ApJ, 652, 1390
Campana, S., et al. 2006, Nature, 442, 1008
Chevalier, R. A. 1992, ApJ, 394, 599
Chevalier, R. A., & Fransson, C. 2008, ApJ, 683, L135
Chiosi, C., & Maeder, A. 1986, ARA&A, 24, 329
Clocchiatti, A., Wheeler, J. C., Brotherton, M. S., Cochran, A. L., Wills, D., Barker, E. S., & Turatto, M. 1996, ApJ, 462, 462
Cohen, M., Wheaton, W. A., & Megeath, S. T. 2003, AJ, 126, 1090
Crowther, P. A. 2007, ARA&A, 45, 177
Cushing, M. C., Vacca, W. D., & Rayner, J. T. 2004, PASP, 116, 362
D'Alessio, V., Piro, L., & Rossi, E. M. 2006, A&A, 460, 653
De Pasquale, M., et al. 2003, ApJ, 592, 1018
Dessart, L., Burrows, A., Livne, E., & Ott, C. D. 2008, ApJ, 673, L43
Dessart, L., & Hillier, D. J. 2008, MNRAS, 383, 57
Di Carlo, E., et al. 2008, ApJ, 684, 471
Dickey, J. M., & Lockman, F. J. 1990, ARA&A, 28, 215
Elmhamdi, A., Danziger, I. J., Cappellaro, E., Della Valle, M., Gouiffes, C., Phillips, M. M., & Turatto, M. 2004, A&A, 426, 963
Ensman, L., & Burrows, A. 1992, ApJ, 393, 742
Faber, S. M., et al. 2003, Proc. SPIE, 4841, 1657
Fabricant, D., Cheimets, P., Caldwell, N., & Geary, J. 1998, PASP, 110, 79
Falco, E. E., et al. 1999, PASP, 111, 438
Fesen, R. A., et al. 2006, ApJ, 645, 283
Filippenko, A. V. 1982, PASP, 94, 715
Filippenko, A. V. 1991, in IAU Symp. 143, Wolf–Rayet Stars and Interrelations with Other Massive Stars in Galaxies, ed. K. A. van der Hucht & B. Hidayat (Dordrecht: Kluwer), 529
Filippenko, A. V. 1997, ARA&A, 35, 309
Filippenko, A. V. 2005, in ASP Conf. Ser. 332, The Fate of the Most Massive Stars, ed. R. Humphreys & K. Stanek (San Francisco, CA: ASP), 33
Filippenko, A. V., Li, W. D., Treffers, R. R., & Modjaz, M. 2001, in ASP Conf. Ser. 246, IAU Colloq. 183: Small Telescope Astronomy on Global Scales, ed. B. Paczynski, W.-P. Chen, & C. Lemme (San Francisco, CA: ASP), 121
Filippenko, A. V., & Sargent, W. L. W. 1986, AJ, 91, 691
Filippenko, A. V., et al. 1995, ApJ, 450, L11
Fisher, A., Branch, D., Hatano, K., & Baron, E. 1999, MNRAS, 304, 67
Fitzpatrick, E. L. 1999, PASP, 111, 63
Foley, R. J., et al. 2006, ApJ, 645, 450
Foley, R. J., Smith, N., Ganeshalingam, M., Li, W., Chornock, R., & Filippenko, A. V. 2007, ApJ, 657, L105
Fransson, C., & Chevalier, R. A. 1987, ApJ, 322, L15
Fukugita, M., Shimasaku, K., & Ichikawa, T. 1995, PASP, 107, 945
Galama, T. J., et al. 1998, Nature, 395, 670
Garg, A., et al. 2007, AJ, 133, 403
Gehrels, N., et al. 2004, ApJ, 611, 1005
Gerardy, C. L., et al. 2004, in Cosmic Explosions in Three Dimensions, ed. P. Höflich, P. Kumar, & J. C. Wheeler (Cambridge: Cambridge Univ. Press), 57
Gezari, S., et al. 2008, ApJ, 683, L131
Ghisellini, G., Ghirlanda, G., & Tavecchio, F. 2007, MNRAS, 382, L77
Hamann, W.-R., Gräfener, G., & Liermann, A. 2006, A&A, 457, 1015
Hamuy, M., et al. 2002, AJ, 124, 417

Hamuy, M., Suntzeff, N. B., Gonzalez, R., & Martin, G. 1988, AJ, 95, 63
Harkness, R. P., et al. 1987, ApJ, 317, 355
Haynes, M. P., Giovanelli, R., Herter, T., Vogt, N. P., Freudling, W., Maia, M. A. G., Salzer, J. J., & Wegner, G. 1997, AJ, 113, 1197
Heise, J., in't Zand, J., Kippen, R. M., & Woods, P. M. 2001, in Gamma-ray Bursts in the Afterglow Era, ed. E. Costa, F. Frontera, & J. Hjorth (Berlin: Springer), 16
Herald, J. E., Hillier, D. J., & Schulte-Ladbeck, R. E. 2001, ApJ, 548, 932
Herbig, G. H. 1975, ApJ, 196, 129
Hicken, M., et al. 2009, ApJ, 700, 331
Hjorth, J., et al. 2003, Nature, 423, 847
Hook, I., et al. 2003, Proc. SPIE, 4841, 1645
Horne, K. 1986, PASP, 98, 609
Immler, E., et al. 2008a, GCN Circ. 7168
Immler, E., et al. 2008b, GCN Circ. 7185
Kasen, D., Thomas, R. C., & Nugent, P. 2006, ApJ, 651, 366
Katz, B., Budnik, R., & Waxman, E. 2009, arXiv:0902.4708
Kong, E., & Maccarone, T. J. 2008, ATEL 1355
Kong, E., et al. 2008a, GCN Circ. 7171
Kong, E., et al. 2008b, GCN Circ. 7164
Landolt, A. U. 1992, AJ, 104, 340
Leibundgut, B., Kirshner, R. P., Pinto, P. A., Rupen, M. P., Smith, R. C., Gunn, J. E., & Schneider, D. P. 1991, ApJ, 372, 531
Leonard, D. C., & Filippenko, A. V. 2005, in ASP Conf. Ser. 342, Supernovae as Cosmological Lighthouses, ed. M. Turatto et al. (San Francisco, CA: ASP), 330
Li, L.-X. 2008, MNRAS, 388, 603
Li, H., & McCray, R. 1992, ApJ, 387, 309
Li, W., Chornock, R., Foley, R. J., Filippenko, A. V., Modjaz, M., Poznanski, D., & Bloom, J. S. 2008, GRB Coordinates Network, 7176, 1
Li, W., & Filippenko, A. V. 2008, Central Bureau Electronic Telegrams, 1202, 3
Li, W., et al. 2001, PASP, 113, 1178
Li, W., Jha, S., Filippenko, A. V., Bloom, J. S., Pooley, D., Foley, R. J., & Perley, D. A. 2006, PASP, 118, 37
Lucy, L. B. 1991, ApJ, 383, 308
Maeda, K., et al. 2008, Science, 319, 1220
Maeda, K., Nomoto, K., Mazzali, P. A., & Deng, J. 2006, ApJ, 640, 854
Maeda, K., et al. 2007, ApJ, 666, 1069
Malesani, D., et al. 2009, ApJ, 692, L84
Malesani, D., et al. 2004, ApJ, 609, L5
Malesani, D., et al. 2008, GCN Circ. 7169
Marion, G. H., Hoeflich, P., Gerardy, C. L., Vacca, W. D., Wheeler, J. C., & Robinson, E. L. 2009, AJ, in press (arXiv:0906.4085)
Matheson, T., Filippenko, A. V., Ho, L. C., Barth, A. J., & Leonard, D. C. 2000a, AJ, 120, 1499
Matheson, T., Filippenko, A. V., Li, W., Leonard, D. C., & Shields, J. C. 2001, AJ, 121, 1648
Matheson, T., et al. 2000b, AJ, 120, 1487
Mazzali, P. A., & Lucy, L. B. 1998, MNRAS, 295, 428
Mazzali, P. A., Deng, J., Maeda, K., Nomoto, K., Filippenko, A. V., & Matheson, T. 2004, ApJ, 614, 858
Mazzali, P. A., et al. 2006, Nature, 442, 1018
Mazzali, P. A., et al. 2005, Science, 308, 1284
Mazzali, P. A., et al. 2008, Science, 321, 1185
Miknaitis, G., et al. 2007, ApJ, 666, 674
Milisavljevic, D., Fesen, R., Gerardy, C., Kirshner, R., & Challis, P. 2009, arXiv:0904.4256
Millard, J., et al. 1999, ApJ, 527, 746
Miller, J. S., & Stone, R. P. S. 1993, Lick Obs. Tech. Rep. 66 (Santa Cruz, CA: Lick Obs.)
Mirabal, N., Halpern, J. P., An, D., Thorstensen, J. R., & Terndrup, D. M. 2006, ApJ, 643, L99
Modjaz, M. 2007, PhD thesis, Harvard Univ.
Modjaz, M., Chornock, R., Foley, R. J., Filippenko, A. V., Li, W., & Stringfellow, G. 2008a, Central Bureau Electronic Telegrams, 1222, 1
Modjaz, M., et al. 2008b, AJ, 135, 1136
Modjaz, M., Kirshner, R. P., Blondin, S., Challis, P., & Matheson, T. 2008c, ApJ, 687, L9
Modjaz, M., Li, W., Filippenko, A. V., King, J. Y., Leonard, D. C., Matheson, T., Treffers, R. R., & Riess, A. G. 2001, PASP, 113, 308
Modjaz, M., et al. 2006, ApJ, 645, L21
Mould, J. R., et al. 2000, ApJ, 529, 786
Mulchaey, J., & Gladders, M. 2005, LDSS-3 User's Guide (Pasadena: Carnegie Observatories) (http://www.lco.cl/telescopes-information/magellan/instruments/ldss-3/ldss-3-users-guide/users-guide)
Nakano, S., Kadota, K., Itagaki, K., & Corelli, P. 2008, IAU Circ., 8908, 2
Nomoto, K., Iwamoto, K., & Suzuki, T. 1995, Phys. Rep., 256, 173
Oke, J. B., et al. 1995, PASP, 107, 375
Page, K. L., et al. 2008, GCN Report 110.1
Patat, F., et al. 2001, ApJ, 555, 900
Phillips, M. M. 1993, ApJ, 413, L105
Phillips, A. C., & Davis, L. E. 1995, in ASP Conf. Ser. 77, Astronomical Data Analysis Software and Systems IV, ed. R. A. Shaw, H. E. Payne, & J. J. E. Hayes (San Francisco, CA: ASP), 297
Pian, E., et al. 2006, Nature, 442, 1011
Podsiadlowski, P., Langer, N., Poelarends, A. J. T., Rappaport, S., Heger, A., & Pfahl, E. 2004, ApJ, 612, 1044
Poole, T. S., et al. 2008, MNRAS, 383, 627
Pooley, D., & Soderberg, A. 2008, GCN Circ. 7216
Predehl, P., & Schmitt, J. H. M. M. 1995, A&A, 293, 889
Quimby, R. M., Wheeler, J. C., Höflich, P., Akerlof, C. W., Brown, P. J., & Rykoff, E. S. 2007, ApJ, 666, 1093
Rayner, J. T., Toomey, D. W., Onaka, P. M., Denault, A. J., Stahlberger, W. E., Vacca, W. D., Cushing, M. C., & Wang, S. 2003, PASP, 115, 362
Rest, A., et al. 2005, ApJ, 634, 1103
Richardson, D. 2009, AJ, 137, 347
Richardson, D., Branch, D., & Baron, E. 2006, AJ, 131, 2233
Richmond, M. W., Treffers, R. R., Filippenko, A. V., Paik, Y., Leibundgut, B., Schulman, E., & Cox, C. V. 1994, AJ, 107, 1022
Riess, A. G., et al. 1998, AJ, 116, 1009
Roming, P. W. A., et al. 2005, Space Sci. Rev., 120, 95
Sakamoto, T., et al. 2008, ApJ, 679, 570
Sakamoto, T., et al. 2005, ApJ, 629, 311
Sauer, D. N., Mazzali, P. A., Deng, J., Valenti, S., Nomoto, K., & Filippenko, A. V. 2006, MNRAS, 369, 1939
Schawinski, K., et al. 2008, Science, 321, 223
Schechter, P. L., Mateo, M., & Saha, A. 1993, PASP, 105, 1342
Scheck, L., Kifonidis, K., Janka, H.-T., & Müller, E. 2006, A&A, 457, 963
Schmidt, B. P., et al. 1993, Nature, 364, 600
Schmidt, G. D., Weymann, R. J., & Foltz, C. B. 1989, PASP, 101, 713
Skrutskie, M. F., et al. 2006, AJ, 131, 1163
Smith, N., & Conti, P. S. 2008, ApJ, 679, 1467
Smith, N., Foley, R. J., & Filippenko, A. V. 2008, ApJ, 680, 568
Smith, N., & Owocki, S. P. 2006, ApJ, 645, L45
Soderberg, A., et al. 2008a, GRB Coordinates Network, 7165, 1
Soderberg, A. M., et al. 2008b, Nature, 453, 469
Soderberg, A. M., et al. 2006, Nature, 442, 1014
Sollerman, J., Leibundgut, B., & Spyromilio, J. 1998, A&A, 337, 207
Sollerman, J., et al. 2006, A&A, 454, 503
Spyromilio, J. 1991, MNRAS, 253, 25P
Spyromilio, J. 1994, MNRAS, 266, L61
Stanek, K. Z., et al. 2003, ApJ, 591, L17
Stritzinger, M., et al. 2002, AJ, 124, 2100
Tanaka, M., et al. 2009, ApJ, 692, 1131
Taubenberger, S., et al. 2006, MNRAS, 371, 1459
Taubenberger, S., et al. 2009, MNRAS, 397, 677
Thöne, C. C., Michałowski, M. J., Leloudas, G., Cox, N. L. J., Fynbo, J. P. U., Sollerman, J., Hjorth, J., & Vreeswijk, P. M. 2009, ApJ, 698, 1307
Tominaga, N., et al. 2005, ApJ, 633, L97
Tomita, H., et al. 2006, ApJ, 644, 400
Uomoto, A., & Kirshner, R. P. 1986, ApJ, 308, 685
Vacca, W. D., Cushing, M. C., & Rayner, J. T. 2003, PASP, 115, 389
Valenti, S., et al. 2008a, GRB Coordinates Network, 7171, 1
Valenti, S., et al. 2008b, Central Bureau Electronic Telegrams, 1205, 1
Vogt, S. S., et al. 1994, Proc. SPIE, 2198, 362
Wade, R. A., & Horne, K. 1988, ApJ, 324, 411
Wang, C., Lai, D., & Han, J. L. 2006, ApJ, 639, 1007
Wang, X.-Y., Li, Z., Waxman, E., & Mészáros, P. 2007, ApJ, 664, 1026
Waxman, E., Mészáros, P., & Campana, S. 2007, ApJ, 667, 351
Wheeler, J. C., et al. 1993, ApJ, 417, L71
Wood-Vasey, W. M., et al. 2008, ApJ, 689, 377
Woosley, S. E., & Bloom, J. S. 2006, ARA&A, 44, 507
Woosley, S. E., Langer, N., & Weaver, T. A. 1993, ApJ, 411, 823
Woosley, S. E., Pinto, P. A., Martin, P. G., & Weaver, T. A. 1987, ApJ, 318, 664
Xu, D., Watson, D., Fynbo, J., Fan, Y., Zou, Y.-C., & Hjorth, J. 2008, in COSPAR, Plenary Meeting, 37th COSPAR Scientific Assembly, 3512